Acoustic oscillations of rapidly rotating polytropic stars

II. Effects of the Coriolis and centrifugal accelerations

D. Reese, F. Lignières, and M. Rieutord

Laboratoire d'Astrophysique de Toulouse et Tarbes - UMR 5572 - Université Paul Sabatier Toulouse 3 - Observatoire Midi-Pyrénées, 14 avenue É. Belin, 31400 Toulouse, France

Abstract

Context. With the launch of space missions devoted to asteroseismology (like COROT), the scientific community will soon have accurate measurements of pulsation frequencies in many rapidly rotating stars.
Aims. The present work focuses on the effects of rotation on pulsations of rapidly rotating stars when both the Coriolis and centrifugal accelerations require a non-perturbative treatment.
Methods. We develop a 2-dimensional spectral numerical approach which allows us to compute acoustic modes in centrifugally distorted polytropes including the full influence of the Coriolis force. This method is validated through comparisons with previous studies, and the results are shown to be highly accurate.
Results. In the frequency range considered and with COROT's accuracy, we establish a domain of validity for perturbative methods, thus showing the need for complete calculations beyond $v \cdot \sin i = 50\,\mathrm{km.s^{-1}}$ for a $R = 2.3\,R_\odot$, $M = 1.9\,M_\odot$ polytropic star. Furthermore, it is shown that the main differences between complete and perturbative calculations come essentially from the centrifugal distortion.

1. Introduction

The study of rapidly rotating stars is a field in which there are many unresolved questions. The structure of these stars, the rotation profile, the angular momentum transport and many other aspects are not well understood. In order to answer some of these questions, many different theoretical and observational methods have been developed over the years. For instance, interferometry is starting to give clues as to the shape of these stars and effects such as gravitational darkening (*e.g.* Domiciano de Souza et al., 2003, 2005, Peterson et al., 2006). On the theoretical side, there exists a number of numerical models which are progressively becoming more realistic (*e.g.* Roxburgh, 2004, Jackson et al., 2005, Rieutord et al., 2005, Rieutord, 2006). These models can then be supplemented with asteroseismology which relates the internal structure to observable stellar pulsations. In order to fully exploit these pulsations, it is necessary to accurately quantify how they are affected by rotation. In the present work, we will show how this can be done for acoustic pulsations in uniformly rotating polytropic stellar models.

Rotation has several effects on stars and their pulsations. These result from the apparition of two inertial forces, namely the centrifugal and the Coriolis forces. The centrifugal force distorts the shape of the star and modifies its equilibrium structure. The Coriolis force intervenes directly in the oscillatory motions. Neither of these effects respect spherical geometry, which means that the radial coordinate r and the colatitude θ are no longer separable. As a result, pulsation modes cannot be described by a single spherical harmonic as was the case for non-rotating stars. In order to tackle this problem, two basic approaches have been developed. The first one is the perturbative approach and applies to small rotation rates. In this approach, both the equilibrium structure and the pulsation mode are the sum of a spherical solution (or a single spherical harmonic), a perturbation, and a remainder which is neglected. The second approach consists in solving directly the 2-dimensional eigenvalue problem fully including the effects of rotation.

Historically, the perturbative method has been applied to first, second and third order. Previous studies include Saio (1981), Gough & Thompson (1990), and Dziembowski & Goode (1992) for second order methods and Soufi et al. (1998) and Karami et al. (2005) for third order methods. These have been applied to polytropic models (Saio, 1981) and then to more realistic models. There have also been some studies based on the non-perturbative approach. Most non-perturbative calculations have focused on the stability of neutron stars, r-modes and f-modes rather than on p-modes. Some exceptions are Clement (1981, 1984, 1986, 1989, 1998), Yoshida & Eriguchi (2001) and Espinosa et al. (2004).

The present work aims at accurately taking into account the effects of rotation on stellar acoustic pulsations, so as to be able to deduce asteroseismological information from rapidly rotating stars. Previous results are either inaccurate or not valid for high enough rotation rates. In order to achieve a sufficient degree of precision, we used numerical methods which have already proved to be highly accurate for other similar problems. The present method is a further development of the numerical method of Lignières et al. (2006b) and Lignières et al. (2006a) (hereafter Paper I) who used a spectral method (Canuto et al., 1988) with a surface-fitting spheroidal coordinate system based on Bonazzola et al. (1998). The spectral method itself has already been used for calculating inertial waves in spherical shells (Rieutord & Valdettaro, 1997) and gravito-inertial modes in a $1.5\,M_\odot$ ZAMS star (Dintrans & Rieutord, 2000) both of which involve the non-perturbative effects of the Coriolis force. Achieving high precision is of great importance for interpreting present and future measurements of stellar pulsations. Furthermore, it provides a means to establish the domain of validity of perturbative methods. Finally, this work can then be used as a reference to validate future methods.

The organisation of the paper is as follows: in the next section, the numerical method is described in detail. This section is followed by a series of comparisons and tests which establish the accuracy of the results. We then proceed to discuss perturbative methods and their validity. A conclusion and outlooks follow.

2. Formalism

The calculation of oscillation modes of rotating polytropes takes place in two steps. Firstly, an equilibrium model must be determined. Secondly, this model needs to be perturbed so as to give the eigenoscillations.

2.1. Equilibrium model

The equilibrium model is a self-gravitating uniformly rotating polytrope described by the following equations in the rotating frame:

$$P_o = K\rho_o^\gamma, \tag{1}$$

$$0 = -\boldsymbol{\nabla}P_o - \rho_o\boldsymbol{\nabla}\left(\Psi_o - \frac{1}{2}\Omega^2 s^2\right), \tag{2}$$

$$\Delta\Psi_o = 4\pi G\rho_o, \tag{3}$$

where P_o is the pressure, ρ_o the density, K the polytropic constant, γ the polytropic exponent, Ψ_o the gravitational potential, s the distance to the rotation axis and G the gravitational constant. One can also introduce the polytropic index $N = 1/(\gamma - 1)$ and a (pseudo-)enthalpy $h = \int \mathrm{d}P/\rho = (1 + N)P_o/\rho_o$. The pressure and density profiles are then proportional to powers of this enthalpy: $P_o \propto h^{N+1}$, and $\rho_o \propto h^N$. A number of non-dimensional parameters also intervene and characterise the polytropic model:

$$\Lambda = \frac{4\pi G\rho_c R_{\mathrm{eq}}^2}{h_c}, \qquad \Omega_\star = \frac{\Omega R_{\mathrm{eq}}}{\sqrt{h_c}}, \qquad \alpha = \frac{\rho_c}{\langle\rho\rangle}, \qquad \varepsilon = 1 - \frac{R_{\mathrm{pol}}}{R_{\mathrm{eq}}}, \tag{4}$$

where quantities with the subscript "c" denote the equilibrium value at the centre of the polytrope, R_{eq} and R_{pol} are the equatorial and polar radii, resp., and $\langle\rho\rangle = 3M/4\pi R_{\mathrm{eq}}^3$ a pseudo-mean density. The method used to compute the equilibrium model is described in Paper I.

2.2. Perturbation equations

We calculate adiabatic, inviscid oscillation modes using Eulerian perturbations to the equilibrium quantities[1]. The linearised equations in the rotating frame read:

$$\partial_t\rho = -\boldsymbol{\nabla}\cdot(\rho_o\boldsymbol{v}), \tag{5}$$

---

[1] The term "perturbation", which means a small departure from equilibrium in this context, is not to be confused with perturbation from the perturbative method, where it means a small departure from the spherical case.

$$\rho_o \partial_t \boldsymbol{v} = -\boldsymbol{\nabla} p + \rho \boldsymbol{g}_o - \rho_o \boldsymbol{\nabla} \Psi - 2\rho_o \boldsymbol{\Omega} \times \boldsymbol{v}, \tag{6}$$

$$\partial_t p - c_o^2 \partial_t \rho = \frac{\rho_o N_o^2 c_o^2}{\|\boldsymbol{g_o}\|^2} \boldsymbol{v} \cdot \boldsymbol{g}_o, \tag{7}$$

$$0 = \Delta \Psi - 4\pi G \rho, \tag{8}$$

where quantities with the subscript "o" denote equilibrium quantities and those without any subscript Eulerian perturbations. $\boldsymbol{g}_o$ is the effective gravity, c_o is the speed of sound, Γ_1 the adiabatic exponent and N_o the Brunt-Väisälä frequency. These are given by the following formulas:

$$\boldsymbol{g}_o = -\boldsymbol{\nabla} \left(\Psi_o - \frac{1}{2}\Omega^2 s^2 \right), \tag{9}$$

$$c_o^2 = \Gamma_1 P_o / \rho_o, \tag{10}$$

$$\Gamma_1 = \left(\frac{\partial \ln p}{\partial \ln \rho} \right)_{ad}, \tag{11}$$

$$N_o^2 = \boldsymbol{g_o} \cdot \left(-\frac{1}{\Gamma_1} \frac{\boldsymbol{\nabla} P_o}{P_o} + \frac{\boldsymbol{\nabla} \rho_o}{\rho_o} \right). \tag{12}$$

It is worth noting that we have used the fluid's barotropicity in the definition of N_o.

We can then put these equations in non-dimensional form using the following transformations:

$$\begin{aligned} t &= T_r \underline{t}, & \rho &= \rho_c \underline{\rho}, & \boldsymbol{r} &= R_{\mathrm{eq}} \underline{\boldsymbol{r}}, & \boldsymbol{g} &= g_r \underline{\boldsymbol{g}}, & \boldsymbol{v} &= V_r \underline{\boldsymbol{v}}, \\ p &= P_r \underline{p}, & \Omega &= \omega_r \underline{\Omega}, & c_o &= V_r \underline{c}_o, & N_o &= \omega_r \underline{N}_o, \end{aligned} \tag{13}$$

where:

$$\omega_r = T_r^{-1} = (4\pi G \rho_c)^{1/2}, \qquad V_r = \frac{R_{\mathrm{eq}}}{T_r}, \qquad g_r = \frac{R_{\mathrm{eq}}}{T_r^2} = 4\pi G R_{\mathrm{eq}} \rho_c, \qquad P_r = \frac{\rho_c R_{\mathrm{eq}}^2}{T_r^2}. \tag{14}$$

It is important to note that $\Omega_\star$ and $\underline{\Omega}$ correspond to two different dimensionless expressions of the rotation rate. In order to go from one expression to the other, one can use the following formula:

$$\Omega_\star = \underline{\Omega} \sqrt{\Lambda}, \tag{15}$$

where Λ is given by Eq. (4).

If we assume a time dependence of the form $\exp(\lambda \underline{t})$, the following generalised eigenvalue problem is obtained (we have dropped the underlined notation):

$$\lambda \rho = -\boldsymbol{v} \cdot \boldsymbol{\nabla} \rho_o - \rho_o \boldsymbol{\nabla} \cdot \boldsymbol{v}, \tag{16}$$

$$\lambda \rho_o \boldsymbol{v} = -\boldsymbol{\nabla} p + \rho \boldsymbol{g}_o - \rho_o \boldsymbol{\nabla} \Psi - 2\rho_o \Omega \boldsymbol{e}_z \times \boldsymbol{v}, \tag{17}$$

$$\lambda p - \lambda c_o^2 \rho = \frac{\rho_o N_o^2 c_o^2}{\|\boldsymbol{g_o}\|^2} \boldsymbol{v} \cdot \boldsymbol{g}_o, \tag{18}$$

$$0 = \Delta \Psi - \rho. \tag{19}$$

2.3. Change of variables

In order to have solutions with a good numerical behaviour on the surface of the star, we use the following variables:

$$\Pi = \frac{p}{H^N}, \qquad b = \frac{\rho}{H^{N-1}}, \tag{20}$$

where $H = h_o / h_c$ is a non-dimensional form of the enthalpy. These choices result from an analysis of the behaviour of the solution near the surface, based on a "generalised" Frobenius study of the system of equations. Although not fully proved, this study gives the correct results in the spherical case (see Appendix A). It also leads to the following boundary condition on the stellar surface:

$$\delta p / \rho_o = 0, \tag{21}$$

where δp is the Lagrangian pressure perturbation. Not only is this result in agreement with previous results, but it also specifies how fast δp goes to zero near the stellar surface. More details on this method are given in Appendix A.

This new choice of variables leads to the following set of equations:

$$\lambda b = -N\boldsymbol{v} \cdot \boldsymbol{\nabla} H - H\boldsymbol{\nabla} \cdot \boldsymbol{v}, \tag{22}$$

$$\lambda H \boldsymbol{v} = -H\left(\boldsymbol{\nabla}\Pi + \boldsymbol{\nabla}\Psi\right) + \boldsymbol{\nabla}H\left(-N\Pi + \frac{b}{\Lambda}\right) - 2\Omega H \boldsymbol{e}_z \times \boldsymbol{v}, \tag{23}$$

$$\lambda\Pi - \lambda\frac{\Gamma_1}{(N+1)\Lambda}b = \left(\frac{\Gamma_1}{\gamma} - 1\right)\frac{\boldsymbol{v} \cdot \boldsymbol{\nabla}H}{\Lambda}, \tag{24}$$

$$0 = \Delta\Psi - H^{N-1}b. \tag{25}$$

If $\Gamma_1 = \gamma$ then $N_o^2 = 0$ and the above system reduces to:

$$\lambda N\Lambda\Pi = -N\boldsymbol{v} \cdot \boldsymbol{\nabla} H - H\boldsymbol{\nabla} \cdot \boldsymbol{v}, \tag{26}$$

$$\lambda\boldsymbol{v} = -\boldsymbol{\nabla}\Pi - \boldsymbol{\nabla}\Psi - 2\Omega\boldsymbol{e}_z \times \boldsymbol{v}, \tag{27}$$

$$0 = \Delta\Psi - N\Lambda H^{N-1}\Pi. \tag{28}$$

This simplification occurs when the polytropic relation (1) is also the equation of state, a situation typical of white dwarfs or neutron stars. Furthermore, both Π and b become proportional to the Eulerian perturbation of the enthalpy, thus justifying *a posteriori* the choice of these variables. As a result, apart from a few multiplicative factors, and the lack of a dissipative force, this second set of equations corresponds to those obtained by Yoshida & Eriguchi (1995).

2.4. Domains and boundary/interface conditions

In order to complete the eigenvalue problem given by Eqs. (22)-(25), it is necessary to specify a number of boundary conditions. The basic requirements are that the solutions remain bounded at the surface and at the centre of the star, and that the gravity potential goes to zero at infinity.

At the centre of the star, the regularity conditions are classically expressed in terms of spherical harmonics (see Eqs. (53) and (54)). By using the variables Π and b from the generalised Frobenius study, the solution is naturally bounded on the star's surface. However, the use of these variables leads to a degeneracy between Eqs. (22), (24) and the radial component of Eq. (23) on the surface of the star. This problem is remedied by replacing the radial component of Eq. (23) with its radial derivative on the surface.

It is also necessary to impose a boundary condition on the perturbation to the gravity potential Ψ, in order to ensure that the potential goes to zero at infinity. Traditionally, this is done by doing a harmonic decomposition of Ψ and imposing the correct condition on each component. However, such a procedure becomes complicated on a spheroidal surface, and it is not certain whether the decomposition of Ψ will converge for highly flattened configurations (Hachisu et al., 1982). We therefore employ a different method based on Bonazzola et al. (1998). It consists in adding a second domain V_2 which is bounded on the inside by the star's surface and on the outside by a sphere of radius $r = 2$ (which is twice the equatorial radius). We solve Poisson's equation in this domain and impose the correct boundary condition on its outer boundary (where we can safely apply a harmonic decomposition). On the inner boundary, it is necessary to use interface conditions which ensure the continuity of Ψ and its radial derivative across the stellar surface.

2.5. Spheroidal geometry

The next step in the calculations is the choice of a coordinate system based on Bonazzola et al. (1998) for each domain. In order to preserve spectral accuracy, the system of coordinates in the first domain needs to fit the surface of the star, and provide a non-singular transformation in the centre. As in Paper I and Rieutord et al. (2005), we choose the following definition for the radial coordinate ζ, which ensures a good convergence of the numerical method:

$$r(\zeta, \theta) = (1 - \varepsilon)\zeta + \frac{5\zeta^3 - 3\zeta^5}{2}\left(R_s(\theta) - 1 + \varepsilon\right), \tag{29}$$

where ε is the flatness given by Eq. (4), $(r(\zeta, \theta), \theta, \phi)$ are the spherical coordinates corresponding to the point (ζ, θ, ϕ), and $R_s(\theta)$ is the surface of the star. By setting $\zeta = 1$, one obtains $r(1, \theta) = R_s(\theta)$, and the centre $r = 0$ is given by $\zeta = 0$.

In second domain, we used the following definition:

$$r(\zeta, \theta) = 2\varepsilon + (1 - \varepsilon)\zeta + \left(2\zeta^3 - 9\zeta^2 + 12\zeta - 4\right)\left(R_s(\theta) - 1 - \varepsilon\right), \tag{30}$$

where $\zeta \in [1, 2]$. This mapping is chosen so as to insure the continuity of r and r_ζ across the boundary $\zeta = 1$, and so that the surface given by $\zeta = 2$ corresponds to the sphere $r = 2$ (r_ζ denotes $\partial_\zeta r$).
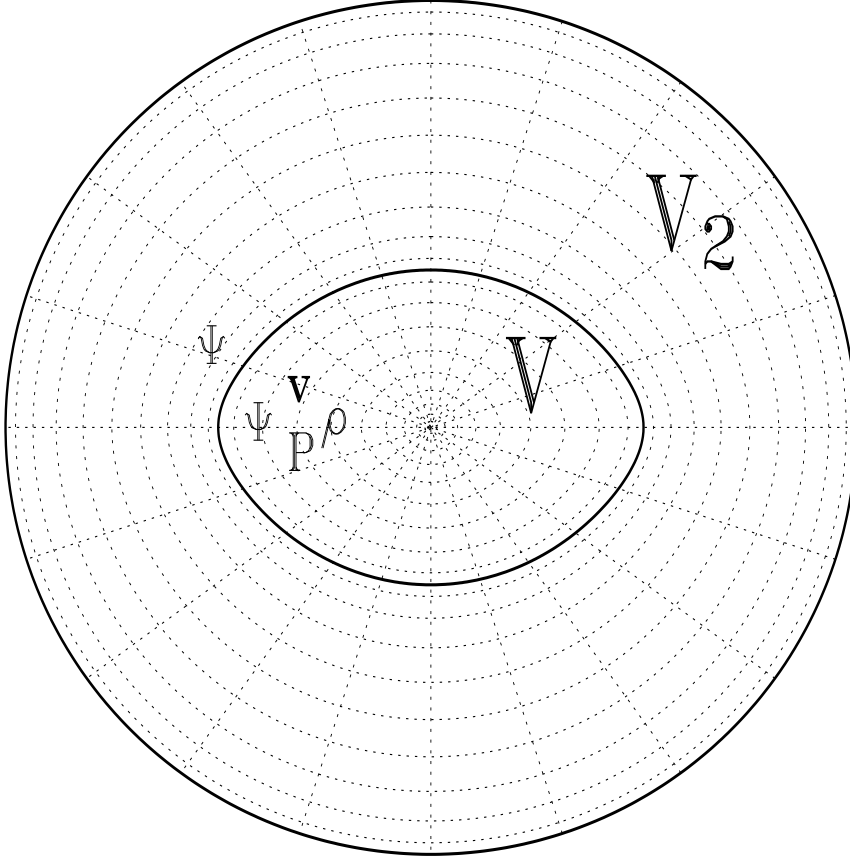
Figure 1. Coordinate system used in computing the equilibrium model of the star and the pulsation modes. The domain V corresponds to the star itself (which in this case is a $N = 3$ polytrope at 84% of the breakup rotation rate). The domain V_2 encompasses the star, its outer limit being a sphere of radius $r = 2$ (twice the equatorial radius). The dotted lines correspond to $\zeta = 0.1, 0.2 \ldots 0.9$ in the domain V, $\zeta = 1.1, 1.2 \ldots 1.9$ in the domain V_2 and $\theta = 0°, 18°, \ldots 342°$. The centre of the star corresponds to $\zeta = 0$, the star's surface (the boundary between V and V_2) to $\zeta = 1$, and the outer boundary to $\zeta = 2$. The continuity equation, Euler's equation, the energy equation and Poisson's equation are solved in the first domain. The letters Ψ, $\boldsymbol{v}$, P and ρ in the domain V show that these variables intervene in the first domain. In the second domain, only Poisson's equation is solved, and only the perturbation of the gravity potential Ψ intervenes. This is represented by the letter Ψ in the domain V_2.

Once the coordinate system has been established, it is also necessary to choose a set of vectors as a basis. We define the following vectors, which are derived from the natural covariant basis $(\boldsymbol{E}_\zeta, \boldsymbol{E}_\theta, \boldsymbol{E}_\phi)$ (defined as $\boldsymbol{E}_i = \partial_i \boldsymbol{r}$):

$$
\begin{aligned}
\boldsymbol{a}_\zeta &= \frac{\zeta^2}{r^2 r_\zeta}\boldsymbol{E}_\zeta && = \frac{\zeta^2}{r^2}\boldsymbol{e}_r, \\
\boldsymbol{a}_\theta &= \frac{\zeta}{r^2 r_\zeta}\boldsymbol{E}_\theta && = \frac{\zeta}{r^2 r_\zeta}\left(r_\theta \boldsymbol{e}_r + r \boldsymbol{e}_\theta\right), \\
\boldsymbol{a}_\phi &= \frac{\zeta}{r^2 r_\zeta \sin\theta}\boldsymbol{E}_\phi && = \frac{\zeta}{r r_\zeta}\boldsymbol{e}_\phi,
\end{aligned}
\tag{31}
$$

where $(\boldsymbol{e}_r, \boldsymbol{e}_\theta, \boldsymbol{e}_\phi)$ are the usual spherical vectors. The vectors $(\boldsymbol{a}_\zeta, \boldsymbol{a}_\theta, \boldsymbol{a}_\phi)$ have been chosen so that they become $(\boldsymbol{e}_r, \boldsymbol{e}_\theta, \boldsymbol{e}_\phi)$ in the spherical limit. Using this base of vectors, we can then express the velocity field as follows:

$$
\boldsymbol{v} = u^\zeta \boldsymbol{a}_\zeta + u^\theta \boldsymbol{a}_\theta + u^\phi \boldsymbol{a}_\phi.
\tag{32}
$$

With these definitions, it is now possible to give an explicit expression of the oscillation equations:

$$
\lambda b = -\frac{N\zeta^2}{r^2 r_\zeta}\left[H_\zeta u^\zeta + \frac{H_\theta u^\theta}{\zeta}\right] - \frac{\zeta^2 H}{r^2 r_\zeta}\left[\partial_\zeta u^\zeta + \frac{2u^\zeta}{\zeta} + \frac{\partial_\theta u^\theta}{\zeta} + \frac{\cot\theta u^\theta}{\zeta} + \frac{\partial_\phi u^\phi}{\zeta \sin\theta}\right],
\tag{33}
$$

$$
\lambda\left[\frac{\zeta^2 H r_\zeta u^\zeta}{r^2} + \frac{\zeta H r_\theta u^\theta}{r^2}\right] = \frac{2\Omega H \zeta \sin\theta u^\phi}{r} - H\left(\partial_\zeta \Pi + \partial_\zeta \Psi\right) + H_\zeta\left(\frac{b}{\Lambda} - N\Pi\right),
\tag{34}
$$

$$
\lambda\left[\frac{\zeta^2 r_\theta u^\zeta}{r^2} + \frac{\zeta(r^2 + r_\theta^2)u^\theta}{r^2 r_\zeta}\right] = \frac{2\Omega\zeta(r_\theta \sin\theta + r\cos\theta)u^\phi}{r r_\zeta} - \partial_\theta \Pi - \partial_\theta \Psi + \frac{H_\theta}{H}\left(\frac{b}{\Lambda} - N\Pi\right),
\tag{35}
$$

$$
\lambda\frac{\zeta u^\phi}{r_\zeta} = -\frac{2\Omega\zeta^2 \sin\theta u^\zeta}{r} - \frac{2\Omega\zeta(r_\theta \sin\theta + r\cos\theta)u^\theta}{r r_\zeta} - \frac{\partial_\phi \Pi}{\sin\theta} - \frac{\partial_\phi \Psi}{\sin\theta},
\tag{36}
$$

$$
\lambda\left(\Pi - \frac{\Gamma_1 b}{(N+1)\Lambda}\right) = \frac{\zeta^2}{\Lambda r^2 r_\zeta}\left(\frac{\Gamma_1}{\gamma} - 1\right)\left[H_\zeta u^\zeta + \frac{H_\theta u^\theta}{\zeta}\right],
\tag{37}
$$

$$0 = \frac{r^2 + r_\theta^2}{r^2 r_\zeta^2}\partial_{\zeta\zeta}^2\Psi + c_\zeta\partial_\zeta\Psi - \frac{2r_\theta}{r^2 r_\zeta}\partial_{\zeta\theta}^2\Psi + \frac{1}{r^2}\Delta_{\theta\phi}\Psi - H^{N-1}b, \tag{38}$$

where:

$$c_\zeta = \frac{1}{r^2 r_\zeta^3}\left(2r_\zeta r_\theta r_{\zeta\theta} - r^2 r_{\zeta\zeta} - r_\zeta^2 r_{\theta\theta} + 2rr_\zeta^2 - r_\theta^2 r_{\zeta\zeta} - r_\zeta^2 r_\theta\cot\theta\right), \tag{39}$$

$$\Delta_{\theta\phi} = \partial_{\theta\theta}^2 + \cot\theta\partial_\theta + \frac{1}{\sin^2\theta}\partial_{\phi\phi}^2. \tag{40}$$

Eq. (33) is the continuity equation, Eqs. (34)-(36) are Euler's equations, Eq. (37) corresponds to the adiabatic energy equation and Eq. (38) is Poisson's equation. Euler's equations have been used in their covariant rather than contravariant form, as it is advantageous from a numerical point of view. In order to understand this, it is helpful to bear in mind that H_θ/H converges towards $H_{\zeta\theta}/H_\zeta$ on the stellar surface, whereas H_ζ/H is unbounded (since $H_\zeta \neq 0$ on the surface). As a result, the radial component of Euler's equation reduces to $b = \Lambda N\Pi$ on the surface (which incidentally is already implied by a linear combination of the energy and continuity equations), whereas the two other components retain useful information on the surface. If the equations where in their contravariant form, than the θ component of Euler's equation would also reduce to $b = \Lambda N\Pi$ on the stellar surface since H_ζ would appear in this equation, thus preventing the possibility of dividing by H. It would then be necessary to also replace this equation by a supplementary boundary condition which would provide the information already contained in the covariant form. This system of equations applies in the first domain, except for Poisson's equation which is used in both domains (of course, the density perturbation no longer appears in the second domain).

2.6. Numerical Method

In order to solve Eqs. (33)-(38), we project these equations onto the spherical harmonics (Rieutord, 1987). This is done in two steps (*c.f.* Paper I). First of all, the different unknowns are expressed in terms of a sum over the spherical harmonics. Explicitly, we obtain:

$$b = \sum_{\ell'=|m|}^{\infty} b_m^{\ell'} Y_{\ell'}^m, \tag{41}$$

$$\Pi = \sum_{\ell'=|m|}^{\infty} \Pi_m^{\ell'} Y_{\ell'}^m, \tag{42}$$

$$\Psi = \sum_{\ell'=|m|}^{\infty} \Psi_m^{\ell'} Y_{\ell'}^m, \tag{43}$$

$$\boldsymbol{v} = \sum_{\ell'=|m|}^{\infty} u_m^{\ell'}\boldsymbol{R}_{\ell'}^m + v_m^{\ell'}\boldsymbol{S}_{\ell'}^m + w_m^{\ell'}\boldsymbol{T}_{\ell'}^m, \tag{44}$$

where $Y_{\ell'}^m$ is the spherical harmonic of degree ℓ' and azimuthal order m and $b_m^{\ell'}$, $\Pi_m^{\ell'}$ etc. are radial functions that need to be determined, and which only depend on ζ. The equilibrium model is axisymmetric meaning that the variable ϕ is not coupled to the two others variables. Therefore, there is no summation over the azimuthal order m in these expressions. However, ζ and θ are not separable since the star does not respect spherical symmetry. As a result, it is necessary to sum over the harmonic degree ℓ'.

$\boldsymbol{R}_{\ell'}^m$, $\boldsymbol{S}_{\ell'}^m$, and $\boldsymbol{T}_{\ell'}^m$ are defined as follows:

$$\boldsymbol{R}_{\ell'}^m = Y_{\ell'}^m\boldsymbol{a}_\zeta, \tag{45}$$
$$\boldsymbol{S}_{\ell'}^m = \partial_\theta Y_{\ell'}^m\boldsymbol{a}_\theta + \mathrm{D}_\phi Y_{\ell'}^m\boldsymbol{a}_\phi, \tag{46}$$
$$\boldsymbol{T}_{\ell'}^m = \mathrm{D}_\phi Y_{\ell'}^m\boldsymbol{a}_\theta - \partial_\theta Y_{\ell'}^m\boldsymbol{a}_\phi, \tag{47}$$
$$\mathrm{D}_\phi \equiv \frac{\partial_\phi}{\sin\theta}. \tag{48}$$

It is worth noting that $\boldsymbol{R}_{\ell'}^m$, $\boldsymbol{S}_{\ell'}^m$, and $\boldsymbol{T}_{\ell'}^m$ are *not* the usual vectorial spherical harmonics because $(\boldsymbol{a}_\zeta, \boldsymbol{a}_\theta, \boldsymbol{a}_\phi)$ is not the same as $(\boldsymbol{e}_r, \boldsymbol{e}_\theta, \boldsymbol{e}_\phi)$. However, in the spherical limit, they will become the usual spherical harmonics. An explicit expression for each component of the velocity reads:

$$u^\zeta = \sum_{\ell'=|m|}^{\infty} Y_{\ell'}^m u_m^{\ell'}, \tag{49}$$

$$u^\theta = \sum_{\ell'=|m|}^{\infty} \partial_\theta Y_{\ell'}^m v_m^{\ell'} + D_\phi Y_{\ell'}^m w_m^{\ell'}, \tag{50}$$

$$u^\phi = \sum_{\ell'=|m|}^{\infty} D_\phi Y_{\ell'}^m v_m^{\ell'} - \partial_\theta Y_{\ell'}^m w_m^{\ell'}. \tag{51}$$

Once the unknown quantities have been expressed this way, the next step is to project the equations themselves onto the spherical harmonic basis. Eqs. (33), (34), (37) and (38) are multiplied by $\{Y_\ell^m\}^*$ and integrated over 4π steradians. For each harmonic degree ℓ of $\{Y_\ell^m\}^*$, a different equation is obtained. The remaining equations are obtained from Eqs. (35) and (36) in a more complicated manner. We compute the integral over 4π radians of $\{$Eq. (35)$\}$ $\{\partial_\theta Y_\ell^m\}^*$ + $\{$Eq. (36)$\}$ $\{D_\phi Y_\ell^m\}^*$ and $\{$Eq. (35)$\}$ $\{D_\phi Y_\ell^m\}^*$ − $\{$Eq. (36)$\}$ $\{\partial_\theta Y_\ell^m\}^*$. This operation corresponds to what would be done in the spherical case (i.e. a projection onto the vectorial spherical harmonics). As a result, the system thus obtained reduces to the classical uncoupled system of equations in the spherical limit. In general, however, this set of equations is a highly coupled system of ordinary differential equations in terms of the radial coordinate ζ, the solution of which gives the unknown radial functions (see Appendix B).

In order to solve this system numerically, we first begin by using a finite number of spherical harmonics $L_{\max}$. The equations are then discretised onto a Gauss-Lobatto collocation grid of $N_r + 1$ points, based on the Chebyshev polynomials. This results in an algebraic system of the form $\mathcal{A}v = \lambda\mathcal{B}v$ in which $\mathcal{A}$ and $\mathcal{B}$ are numerically determined square matrices. The eigensolutions (λ, v) of this system correspond to the frequencies and pulsation modes of the star. They are determined iteratively through the Arnoldi-Chebyshev algorithm (e.g. Chatelin, 1988). The coefficients of matrices $\mathcal{A}$ and $\mathcal{B}$ are computed using an equilibrium model with a harmonic resolution $L_{\mod}$ and a Chebyshev (radial) resolution of $N_r + 1$. They are calculated using the coupling integrals given in Appendix B. This is achieved through Gauss' quadrature method with L_{res} points. Typical values for the different resolutions are: $N_r = 60$, $L_{\mod} = 50$, $L_{\max} = 80$, $L_{res} = 230$.

At this point, we can write the boundary condition on the gravitational potential and the regularity conditions at the centre. The boundary condition is applied along the surface $r_{ext} = 2$ (or $\zeta = 2$) on each harmonic component of the gravitational potential perturbation (Hurley et al., 1966):

$$\frac{1}{1-\varepsilon}\frac{d\Psi_m^\ell}{d\zeta} + \frac{\ell+1}{r_{ext}}\Psi_m^\ell = 0. \tag{52}$$

The regularity condition depends on the parity of ℓ in a solution. Thanks to star's equatorial symmetry, modes will either be described by a sum of spherical harmonics with even degrees or odd degrees[2] (see Sect. 2.7). For modes with even harmonics, we apply the following condition at $r = 0$ (or $\zeta = 0$):

$$\frac{d\Psi_m^\ell}{d\zeta} = 0, \qquad \frac{d\Pi_m^\ell}{d\zeta} = 0, \qquad \frac{db_m^\ell}{d\zeta} = 0, \qquad u_m^\ell = 0, \qquad v_m^\ell = 0, \qquad w_m^\ell = 0. \tag{53}$$

The other modes follow the condition:

$$\Psi_m^\ell = 0, \qquad \Pi_m^\ell = 0, \qquad b_m^\ell = 0, \qquad \frac{du_m^\ell}{d\zeta} = 0, \qquad \frac{dv_m^\ell}{d\zeta} = 0, \qquad \frac{dw_m^\ell}{d\zeta} = 0. \tag{54}$$

2.7. Mode classification and symmetries

A number of useful pieces of information can be deduced from the various symmetries present in the system. These help with mode classification, reduce numerical demand and explain certain properties which were observed in perturbative calculations.

The first and most obvious symmetry stems from the fact that the equilibrium model is axisymmetric. This implies that modes will have a well defined azimuthal order m (as explained earlier on). A second equally obvious symmetry results from the star being symmetric with respect to the equatorial plane. This leads to oscillation modes which are either symmetric or antisymmetric with respect to the equatorial plane and which are called even or odd, respectively. In terms of spherical harmonics, even modes are made up of harmonic components such that $\ell + m$ is even, except for the toroidal component of the velocity field in which $\ell + m$ is odd. Odd modes correspond to the opposite situation. From a numerical point of view, eigensolutions are described with half as many components as solutions with no particular parity.

There are two more symmetries which are a little more subtle than the previous ones. The first one only applies if the Coriolis force is neglected and only shows up in the rotating frame. In this situation, only even powers of the

---

[2] The toroidal components w_m^ℓ have the opposite parity with respect to the other components.

rotation rate show up in the equilibrium and pulsation equations. As a result, a given mode will also only depend on Ω^2 and will be a solution for the rotation rates Ω and $-\Omega$. When this symmetry is combined with the next one, then for a given multiplet, modes with azimuthal orders m and $-m$ have the same frequency, as was already pointed out in Paper I.

The last symmetry applies even with the Coriolis force and for both rotating and non-rotating frames. Let us consider a solution $(\omega, \rho, P, \boldsymbol{v}, \Psi, \Omega, m)$ (we include the rotation rate and the azimuthal order for the sake of clarity) and denote by $\mathcal{S}$ the operator which gives the mirror image with respect to the meridian passing through $\phi = 0$[3]. We then find that $(\omega, \mathcal{S}\rho, \mathcal{S}P, \mathcal{S}\boldsymbol{v}, \mathcal{S}\Psi, -\Omega, -m)$ is also a solution (this is not to be confused with the previous symmetry for which $(\omega, \rho, P, \boldsymbol{v}, \Psi, -\Omega, m)$ was the corresponding solution). This symmetry was pointed out by Clement (1989), however some of its consequences on perturbative calculations were not fully appreciated at the time. Let us consider a perturbative description of two frequencies with the same radial order and harmonic degree but with opposite azimuthal orders. We will obtain expressions of the following form:

$$\omega_{n,\ell,m}(\Omega) = \omega_{n,\ell,m}^0 + \omega_{n,\ell,m}^1\Omega + \omega_{n,\ell,m}^2\Omega^2 + ... + \mathcal{O}\left(\Omega^k\right), \tag{55}$$

$$\omega_{n,\ell,-m}(\Omega) = \omega_{n,\ell,-m}^0 + \omega_{n,\ell,-m}^1\Omega + \omega_{n,\ell,-m}^2\Omega^2 + ... + \mathcal{O}\left(\Omega^k\right), \tag{56}$$

where $\omega_{n,\ell,m}^j$ is the jth perturbative coefficient of $\omega_{n,\ell,m}(\Omega)$. If we apply the symmetry, we find that $\omega_{n,\ell,m}(\Omega) = \omega_{n,\ell,-m}(-\Omega)$. By equating like powers of $\omega_{n,\ell,-m}(-\Omega)$ with $\omega_{n,\ell,m}(\Omega)$, we find that $\omega_{n,\ell,m}^j = (-1)^j\omega_{n,\ell,-m}^j$. Therefore $\omega_{n,\ell,m}^j$ will be an even function of m when j is even and an odd function of m when j is odd. This explains why the second order coefficients of Dziembowski & Goode (1992) were polynomials in m^2, and is also found at third order (Goupil, private communication). This symmetry can also be used to increase the accuracy of least squares estimates of the coefficients based on non-perturbative calculations (see Sect. 4.1.1).

3. Analysis of the accuracy of the results

In order to check whether the results presented here are correct, it is important to do a number of internal tests and comparisons with previous studies. We first begin by discussing the accuracy of the underlying polytropic models. This is then followed by a series of comparisons with other studies. In the two first comparisons, the previous results have a limited accuracy, therefore only allowing a qualitative evaluation. The next two comparisons are with very accurate results, thus allowing a quantitative evaluation of the precision of the present results. These are then followed by a test based on the variational principle and an analysis of the sensitivity of the results to the parameters used in the numerical method. Finally, we conclude by estimating the overall accuracy of the results.

3.1. Accuracy of the polytropic models

There are several different tests which give an idea of the accuracy of the polytropic models. One way is by looking at the effects of different input parameters, such as the radial or harmonic resolution, on various non-dimensional parameters like those in Eq. (4). For non-rotating models, these non-dimensional parameters can be compared with those given in Seidov (2004). In Table 1, we give such a comparison, which shows that it is possible to correctly obtain 6 digits after the decimal point. Table 2 contains α and Λ for an $N = 3$ polytrope rotating at $0.59\,\Omega_K$. This table shows the strong influence of $N_{\rm r}$ and the need for a sufficient radial resolution. It also suggests a precision of 6 digits after the decimal point, if we compare the values for $N_{\rm r} = 50$ and $N_{\rm r} = 60$.

Table 1. Non-dimensional parameters of a non-rotating $N = 3$ polytrope. $L_{\max} = 50$ for all the calculations. It is difficult to accurately obtain the 7th digit after the decimal point, in comparison with the values of Seidov (2004).

$N_{\rm r}$	α	Λ
50	54.182 480 87	47.566 520 74
60	54.182 481 06	47.566 520 85
100	54.182 480 87	47.566 520 74
Seidov (2004)	54.182 481 11	47.566 520 88

---

[3] In spherical coordinates, $\mathcal{S}$ is defined as follows for a scalar quantity: $\mathcal{S}A(r,\theta,\phi) = A(r,\theta,-\phi)$. For a vector field it takes on the definition: $\mathcal{S}\boldsymbol{V}(r,\theta,\phi) = V_r(r,\theta,-\phi)\boldsymbol{e}_r + V_\theta(r,\theta,-\phi)\boldsymbol{e}_\theta - V_\phi(r,\theta,-\phi)\boldsymbol{e}_\phi$.

Table 2. Same as Table 1 but for an $N = 3$ polytrope rotating at $0.59\,\Omega_K$. The radial resolution N_r has a stronger effect on the values of α and Λ than the harmonic resolution L_max.

N_r	L_max	α	Λ
50	16	81.108 265 69	63.025 583 86
20	50	81.108 444 82	63.025 591 55
50	50	81.108 249 13	63.025 575 39
50	60	81.108 249 08	63.025 575 36
60	50	81.108 249 38	63.025 575 52
60	60	81.108 249 38	63.025 575 52

In addition to the previous test, it is also possible to apply the virial theorem to obtain a measure of the accuracy of the model's structure. In what follows we use the following formulation of the theorem:

$$0 = \int_V \rho_o \Omega_\star^2 r^2 \sin^2 \theta dV + \frac{1}{2} \int_V \rho_o \Psi_o dV + \frac{3}{N+1} \int_V P_o dV, \tag{57}$$

where $\rho_o = H^N$, $P_o = H^{N+1}$ and $\Psi_o = \psi_o/h_c$. For a sufficient number of iterations, it is possible to attain a precision of 10^{-13} on the virial test. Beyond this point, successive iterations are useless and can actually decrease the accuracy of the model. In Fig. 2, we follow the evolution of Λ and the virial error with each iteration. As can be seen in the figure, there are two phases: a first phase in which the model is approaching the mathematical solution to the problem, and a second phase in which the maximum precision has been attained and the model is slowly drifting towards less accurate solutions. For some of the rotating configurations and with a well adjusted resolution, this second phase does not contain a slow drift but remains close to a fixed point. Either way, the best point at which to stop the iterative scheme is at the transition between the two phases.
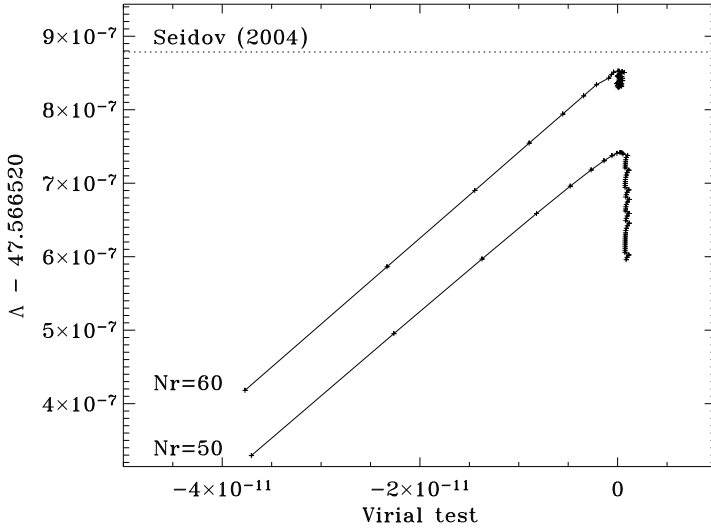
Figure 2. A plot of the value of Λ as a function of the virial error. Each iteration is marked by a plus "+" and connected consecutively. As shown in the figure, the iterated models reach a point of closest approach to the mathematical solution, and then slowly drift towards less accurate models.

The models on which are based the pulsation frequencies do not attain as high a precision, because the iterative scheme was stopped before the transition between the two phases. This is because we use a small parameter called ϵ which controls the relative error on the enthalpy and serves as a stopping criteria. If the value of ϵ is too low, than the iterative program never reaches this precision on the enthalpy and therefore does not output the stellar model. We therefore set $\epsilon = 10^{-8}$ in most calculations, which ensures successful convergence but reduces the accuracy of the model. As a result, the virial test typically attains a precision of 4×10^{-10}. For the non-rotating model, α takes on a value around 54.182473, which starts differing at the 5th digit after the decimal point from the value given in Seidov (2004) and corresponds to a relative precision of $\sim 10^{-7}$.

3.2. Comparison with Saio (1981)

Saio (1981) gives second order perturbative calculations for polytropic models. Based on his coefficients, it is possible to obtain pulsation frequencies via the following formula:

$$\omega = \omega_0 - (1 - C_1)\, m\Omega + \left\{ (X_1 + X_2 + Z) + m^2 (Y_1 + Y_2) \right\} \frac{\Omega^2}{\omega_0}. \tag{58}$$

In order to compare our results with his, it is necessary to extract perturbative coefficients from our own results. The procedure used to find these coefficients is fully described in Sect. 4.1.1. Before applying this procedure, we first had to express our results in the same units as Saio (1981) via the following conversion rule:

$$\omega_{S81} = \sqrt{3\alpha_{nr}}\omega, \tag{59}$$

$$\Omega_{S81} = \sqrt{\frac{3\alpha_{nr}}{\Lambda}}\Omega_\star, \tag{60}$$

where the subscript "nr" means "non-rotating" (*i.e.* the value of the parameter for the non-rotating polytrope) and the subscript "S81" means that the quantity is in Saio's units. It turns out that in Saio's units, the mass of the polytrope depends on the rotation rate. A comparison between his coefficients $\left(\omega_0^2, C_1, X_1 + X_2 + Z, Y_1 + Y_2\right)$ and ours showed a qualitative agreement between the two (to within 2 %). This reduces the possibility of programming errors affecting our results.

3.3. Comparison with Clement (1984)

Further comparisons can be done with Clement (1984), who applied non-perturbative techniques to calculate pulsation frequencies for $N = 1$ and $N = 3$ polytropes. His frequencies are given in the same units as ours and no conversion is needed. However, Clement (1984) used a rotational parameter which he called "α" (denoted here as α_{C84} so as to avoid confusion with α from Eq. (4)) and which is "neither dimensionless nor scale-free". Therefore, based on the conversion given in Tables 1 and 2 of Clement (1984) and following his recommendations, we used the parameter $v = \Omega^2/2\pi G\rho_c$ instead. We allowed for uncertainties in the last digit of v and therefore calculated a corresponding range of frequencies. For example, if $v = 1.69 \times 10^{-2}$ we would calculate the frequencies corresponding to $v = 1.69 \times 10^{-2} \pm 5 \times 10^{-5}$. The results are presented in Fig. 3.
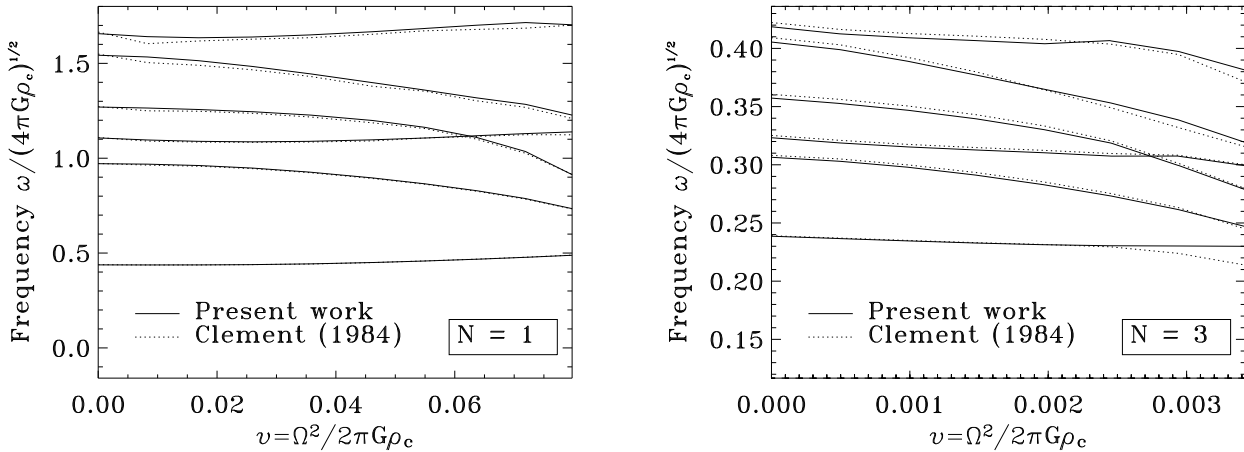
Figure 3. A plot showing the frequencies in Clement (1984) and our calculations of the same frequencies

As can be seen from Fig. 3 the two sets of results qualitatively agree, which once more makes numerical programming mistakes unlikely in our calculations. However, Clement's results usually do not lie in the frequency intervals we calculated (this would require a 4-digit accuracy). This is partially due to the fact that it is difficult to accurately reproduce the polytropic models he used. In order to illustrate this, we can use the different parameters $(v,\ \rho_c/\bar{\rho},\ R_{\mathrm{eq}}/R_{\mathrm{pol}},\ g_e/g_p)$ provided in Tables 1 and 2 of Clement (1984), allow for uncertainties in the last digit, and calculate the corresponding ranges for $\Omega_\star$. For a given rotation rate, if all the digits in the four parameters are accurate, then the four different ranges for $\Omega_\star$ should overlap and give a more precise idea as to the underlying model. However, it was only possible to obtain at most three overlapping ranges, and not four. A typical example for the $N = 1$ polytrope (with $\alpha_{C84} = 0.004$) is:

$$
\begin{aligned}
v &= 3.57 \times 10^{-2} \pm 5 \times 10^{-5} &\Rightarrow \Omega_\star &= 0.4615 \pm 4 \times 10^{-4}, \\
\rho_c/\bar{\rho} &= 3.40 \pm 5 \times 10^{-3} &\Rightarrow \Omega_\star &= 0.4580 \pm 9.4 \times 10^{-3}, \\
R_{\mathrm{eq}}/R_{\mathrm{pol}} &= 1.162 \pm 5 \times 10^{-4} &\Rightarrow \Omega_\star &= 0.4590 \pm 7 \times 10^{-4}, \\
g_e/g_p &= 0.686 \pm 5 \times 10^{-4} &\Rightarrow \Omega_\star &= 0.4621 \pm 4 \times 10^{-4}.
\end{aligned}
\tag{61}
$$

This shows that the error bars we used on Clement's parameters are too small and that the uncertainties on his models are larger. Nonetheless, these uncertainties do not fully account for the discrepancies between our frequencies and his. This can be shown by the fact that even for non-rotating configurations (where there is no ambiguity on the underlying model) the differences are still of the same order of magnitude.

In general, a quantitative comparison between our results and those of Saio (1981) and Clement (1984) showed an agreement to 2 or 3 significant digits. While providing a correct qualitative picture, the precision of these studies is insufficient for future missions such as COROT. COROT will observe pulsation frequencies within the range of $0.1 - 10$ mHz with an accuracy of $0.6\,\mu$Hz for the 20 day runs and $0.08\,\mu$Hz for the 150 day runs (*e.g.* Baglin et al., 2002), meaning that an accuracy of 3 to 5 digits is required. Therefore, it is important to show that our results meet up to this requirement through other more constraining tests and comparisons.

3.4. Comparison with Christensen-Dalsgaard & Mullan (1994)

Christensen-Dalsgaard & Mullan (1994) give very accurate frequencies for several *non-rotating* polytropic models. Comparing our results with theirs provides a robust test for accuracy. In order to convert our frequencies ω into their units, we apply the following conversion rule:

$$\nu_{CDM} = \nu_g \sqrt{3\alpha}\omega, \qquad (62)$$

where ν_{CDM} is our frequency in their units, $\nu_g = 99.855377\,\mu$Hz, and α is given by Eq. (4). A comparison between their frequencies and ours revealed a very good agreement ($\Delta\omega/\omega \sim 10^{-7}$ for a $N = 3$ polytrope and $\Delta\omega/\omega \sim 10^{-8}$ for a $N = 1.5$ polytrope at $\Omega = 0$). The modes which were compared are: $\ell = 0$ to 3, $n = 1$ to 10 for $N = 3$ and $n = 15$ to 25 for $N = 1.5$. The differences come from round-off errors in the last digit (if we keep the same number of significant digits).

3.5. Comparison with Paper I

We finally compared our results with those of Paper I. In order to do this comparison, it is necessary to remove the Coriolis force and to make the Cowling approximation. No conversion rule is necessary since both sets of results are given in the same units. The two sets of frequencies agree quite well, even at large rotation rates ($\Delta\omega/\omega \sim 10^{-7}$). This result is significant due to the fact that the set of equations used in Paper I is entirely different than the one used here.

3.6. Variational test

The variational principle provides an integral formula which relates a pulsation frequency to the structure of the corresponding mode (*e.g.* Lynden-Bell & Ostriker, 1967). It is therefore possible to apply this formula to a numerically calculated eigenmode to obtain a "variational frequency". The error on this frequency is quadratic in the error of the eigenfunction (*c.f.* Christensen-Dalsgaard & Mullan, 1994). By comparing this frequency with the one obtained directly, it is possible to estimate the accuracy of the results. We used the following non-dimensional formulation of the variational principle:

$$\omega^2 \int_V \rho_o |\boldsymbol{v}|^2 dV - |\omega|^2 \left(\int_V \frac{|p|^2 dV}{\rho_o c_o^2} - \int_{V_\infty} |\boldsymbol{\nabla}\Psi|^2\, dV \right) + 2i\omega \int_V \rho_o \boldsymbol{\Omega} \cdot (\boldsymbol{v}^* \times \boldsymbol{v})\, dV - \int_V \rho_o N_o^2 |\boldsymbol{v} \cdot \boldsymbol{e}_g|^2\, dV = 0, \qquad (63)$$

where V is the volume of the star, V_∞ is infinite space, and $\boldsymbol{e}_g$ the unit vector in the same direction as the gravity vector. The pressure is replaced by $H^N\Pi$ and the different integrals are performed numerically[4] which gives a second degree equation in ω. Solving this equation gives the variational frequency which can then be compared with the direct calculation of ω. Generally, we find differences $\Delta\omega/\omega \sim 10^{-8}$ or better between the two. This can be compared with the results of Ipser & Lindblom (1990) who found differences of 10^{-3} when they applied the variational principle to their calculations. An explicit formulation of the variational principle in spheroidal geometry is given in Appendix C.

3.7. Influence of the parameters from the numerical method

A final test consists in modifying different input parameters and seeing the effect it has on the results. We have therefore applied this test to a few modes which are representative of all the modes that have been calculated. The parameters that were modified are the radial resolution N_{r} (which is the same for the equilibrium model and the

---

[4] The numerical integration was based on Gauss' quadrature method and a spectral expansion, using a radial resolution of 101 points and an angular resolution of 200 points.

pulsation mode), the harmonic resolution of the model L_{mod}, the harmonic resolution of the pulsation mode L_{max}, the shift σ used in the Arnoldi-Chebyshev algorithm[5], and ϵ which controls the relative error of the enthalpy in the equilibrium model. Table 3 lists the values used for the different parameters and the induced frequency variations. For a given parameter, we used the frequency obtained at highest resolution (or lowest value for ϵ) as a reference. In most cases, we obtained a rough plateau at the different levels given in Table 3. In some cases however, there was a definite decrease of the error. For instance, for those modes in which it was tested, the error was roughly proportional to ϵ. Also, for high frequency modes, the error strongly decreased as N_{r} increased, as could be expected for high radial orders. In the table, we put the lower/final values of the error for both of these parameters. The information on the shift is slightly different. The line "Values" gives the amplitude of the variation on the value of the shift. The next two lines contain the standard deviation of the results.

The results on ϵ are not representative of the calculated frequencies. As was pointed out in Sect. 3.1, the number iterations was usually less than optimal because of a large value of ϵ (10^{-8} instead of 10^{-10}), thus resulting in a decreased accuracy. The relative error on low frequency modes is 10^{-8} and that of high frequency modes 10^{-7}.

Table 3. Frequencies variations in terms of different parameters. L_{max} is the harmonic resolution of the pulsation modes, L_{mod} the harmonic resolution of the models and N_{r} the radial resolution. The line "Values" gives the different values that were used for the resolutions, ϵ and the width giving the variation of the shift. The two following lines give the order of magnitude of the induced frequency variations (in units of $\sqrt{4\pi G\rho_c}$).

	L_{max}	L_{mod}	N_{r}	Shift	ϵ
Values	40, 44 ... 80	30, 34 ... 70	32, 36 ... 60	$2 - 5 \times 10^{-4}$	$10^{-8}...10^{-10}$
Low frequency modes	$< 10^{-15}$	10^{-10}	10^{-10}	10^{-13}	10^{-10}
High frequency modes	10^{-14}	10^{-9}	10^{-10}	10^{-11}	10^{-9}

3.8. Discussion

Overall, the main source of error in the present calculations is the uncertainties on the equilibrium model. This is because we chose a convergence criteria which was sure to be met, but which lead to a number of iterations less than optimal. This therefore leads to a global accuracy of 7 digits after the decimal point (in units of $\sqrt{4\pi G\rho_c}$), the last digit being uncertain. Table 3 however shows that these calculations could potentially be made more accurate. The present accuracy is nonetheless largely sufficient for the requirements of COROT, which will be at most 5 significant digits.

4. Results

We now proceed to present the results themselves. We followed acoustic adiabatic pulsation modes (with $\Gamma_1 = 5/3$) from a zero rotation rate to $0.59\Omega_K$ (where $\Omega_K = \sqrt{GM/R_{\mathrm{eq}}^3}$ is the Keplerian break-up rotation rate), using the same procedure as in Paper I. This involves identifying the frequencies at $\Omega = 0$, following their evolution while progressively increasing the rotation rate, and working through a number of avoided crossings. The underlying polytropic models have an index $N = 3$ which gives a polytropic exponent $\gamma = 4/3$. The modes that were calculated are: $\ell = 0$ to 3, $n = 1$ to 10 and $m = -\ell$ to ℓ both with and without the Coriolis force.

4.1. Comparison with perturbative methods

In this section, we compare complete and perturbative calculations so as to determine the range of validity of perturbative methods.

4.1.1. Perturbative coefficients

In order to compare perturbative calculations with complete ones, it proved necessary to compute our own perturbative coefficients, since we were unable to find perturbative coefficients for polytropic models with a sufficient accuracy in the literature. Instead of using the traditional method of perturbing the fluid equations and finding corrections of various

---

[5] The shift comes from shift-and-invert methods and corresponds to a trial value around which the Arnoldi-Chebyshev algorithm looks for frequencies. See Valdettaro et al. (2006) for an extensive discussion on the role of the shift in numerical errors.

orders on the frequencies (see Soufi et al. (1998) for a complete description), we did a series of complete calculations for small rotation rates $((\Omega_\star)_i = 0, 10^{-6}, 10^{-5}, 10^{-4}, 10^{-3}, 0.002, 0.004 \ldots 0.018)$ and applied a least squares fit to the results. In order to increase the accuracy of such calculations, we made use of Eq. (55) and separated even and odd powers of the rotation rate:

$$\frac{\omega_{n,l,m} + \omega_{n,l,-m}}{2} = \omega_{n,l,m}^0 + \omega_{n,l,m}^2 \Omega^2 + \omega_{n,l,m}^4 \Omega^4 + \mathcal{O}(\Omega^6), \tag{64}$$

$$\frac{\omega_{n,l,m} - \omega_{n,l,-m}}{2} = \omega_{n,l,m}^1 \Omega + \omega_{n,l,m}^3 \Omega^3 + \omega_{n,l,m}^5 \Omega^5 + \mathcal{O}(\Omega^7). \tag{65}$$

By fitting $(\omega_{n,l,m} + \omega_{n,l,-m})/2$ and $(\omega_{n,l,m} - \omega_{n,l,-m})/2$ the number of unknowns is reduced to three and the residues are smaller. It is necessary to include the fourth and fifth powers of the rotation rate so as to ensure that the second and third order coefficients are reasonably accurate. The results are given in Table 4 for frequencies and rotation rates in units of $\left(GM/R_{\mathrm{pol}}^3\right)$. From these coefficients the frequencies are given through the following formula:

$$\omega = \omega_0 - m(1 - C)\Omega + \left(D_1 + m^2 D_2\right)\Omega^2 + m\left(T_1 + m^2 T_2\right)\Omega^3 + \mathcal{O}\left(\Omega^4\right). \tag{66}$$

The form of the second degree coefficients was obtained from Saio (1981) and that of the third degree coefficients from Goupil (private communication). In order to express these results in units of Ω_K instead, one can use the following perturbative formula:

$$\left(\frac{\Omega}{\Omega_K}\right) = \left(\frac{\Omega}{\Omega_K^{\mathrm{pol}}}\right) + A\left(\frac{\Omega}{\Omega_K^{\mathrm{pol}}}\right)^3 + \mathcal{O}\left\{\left(\frac{\Omega}{\Omega_K^{\mathrm{pol}}}\right)^5\right\}, \tag{67}$$

where $\Omega_K^{\mathrm{pol}} = \left(GM/R_{\mathrm{pol}}^3\right)$ and $A \simeq 0.77166$.

Table 4. Perturbative coefficients for a $N = 3$ polytrope, deduced from complete calculations. The frequencies and the rotation rate are expressed in units of $\left(GM/R_{\mathrm{pol}}^3\right)^{1/2}$.

ω_0	C	D_1	D_2	T_1	ω_0	C	D_1	D_2	T_1	T_2
\multicolumn{5}{c}{$\ell = 0$}	\multicolumn{6}{c}{$\ell = 2$}
3.042155	...	-1.194	...	...	3.906874	0.1538359	-1.578	-0.294	0.02344	0.00527
4.121230	...	-2.315	...	...	5.169469	0.0818188	-2.396	-0.459	0.00493	0.00477
5.336900	...	-3.439	...	...	6.439990	0.0544285	-3.146	-0.606	0.00020	0.00307
6.591212	...	-4.484	...	...	7.708951	0.0403695	-3.867	-0.745	-0.00087	0.00218
7.855027	...	-5.484	...	...	8.975891	0.0318248	-4.572	-0.880	-0.00094	0.00169
9.120432	...	-6.459	...	...	10.240946	0.0260651	-5.267	-1.013	-0.00074	0.00139
10.384948	...	-7.416	...	...	11.504260	0.0219090	-5.955	-1.144	-0.00049	0.00119
11.647767	...	-8.361	...	...	12.765953	0.0187647	-6.636	-1.273	-0.00025	0.00105
12.908679	...	-9.298	...	...	14.026134	0.0163027	-7.314	-1.402	-0.00006	0.00094
14.167704	...	-10.228	...	...	15.284901	0.0143246	-7.987	-1.530	0.00010	0.00086
\multicolumn{5}{c}{$\ell = 1$}	\multicolumn{6}{c}{$\ell = 3$}
3.377036	0.0295367	-1.072	-1.030	-0.04612	4.294602	0.1193654	-1.898	-0.169	-0.01155	0.00041
4.642432	0.0342809	-1.760	-1.699	-0.04204	5.591067	0.0742468	-2.728	-0.240	-0.00113	0.00157
5.909240	0.0335303	-2.402	-2.315	-0.02715	6.878680	0.0517251	-3.496	-0.307	0.00015	0.00140
7.176668	0.0305143	-3.019	-2.901	-0.01634	8.158826	0.0387755	-4.236	-0.371	0.00038	0.00113
8.443277	0.0270732	-3.621	-3.470	-0.00951	9.433911	0.0305232	-4.960	-0.434	0.00043	0.00091
9.708372	0.0238467	-4.213	-4.028	-0.00524	10.705348	0.0248710	-5.674	-0.496	0.00044	0.00076
10.971700	0.0210064	-4.797	-4.578	-0.00254	11.973956	0.0207887	-6.380	-0.557	0.00046	0.00064
12.233222	0.0185621	-5.375	-5.122	-0.00080	13.240238	0.0177183	-7.081	-0.618	0.00048	0.00055
13.492998	0.0164731	-5.950	-5.662	0.00034	14.504529	0.0153345	-7.777	-0.678	0.00050	0.00048
14.751133	0.0146882	-6.521	-6.198	0.00108	15.767068	0.0134359	-8.470	-0.738	0.00051	0.00042

In order to estimate the accuracy of these perturbative coefficients, there are a number of tests that can be done. First of all, the zeroth order coefficients are simply the pulsation frequencies without rotation but are treated as unknowns in the least squares development. The frequencies without rotation are recovered in the least squares fit to an accuracy of at least 5.4×10^{-8} in the units of Table 4. The first order coefficient C, can be calculated via integrals based on the zeroth order solution (Ledoux, 1951). This alternate way of calculating the coefficients agrees to within 1.4×10^{-9} (this does not necessarily mean that the coefficients are accurate to that precision but does show a high

degree of internal coherence). For the second and third degree coefficients, we checked to see if they satisfied the forms given in Eq. (66); the number of significant digits in Table 4 has been adjusted accordingly. These forms were a constraint only on the $\ell = 2$ and 3 second order coefficients and on the $\ell = 3$ third order coefficients. Another test we did consisted in applying the least squares fit to a subset of the results used in the first fit and seeing whether the coefficients were altered. This test indicates roughly the same accuracy as the other tests.

4.1.2. Comparison

Based on these coefficients, it is possible to calculate perturbative frequencies which can then be compared to the complete calculations, thereby establishing a domain of validity for perturbative methods. In Fig. 4, we show two such domains for $3^{\rm rd}$ order methods, one for each of COROT's error bars ($0.6\,\mu$Hz for the 20 runs and $0.08\,\mu$Hz for the 150 day runs). The underlying polytropic models have a fixed mass of $1.9\,M_\odot$ and a fixed polar radius of $2.3\,R_\odot$, both of which are typical of δ Scuti pulsators. When the distance between the perturbative frequency and the complete one exceeds COROT's error bars, the frequency is shown in black. Otherwise, it is shown in grey. From these figures, it is clear that complete methods are required beyond $v \cdot \sin i = 75\,{\rm km.s}^{-1}$ for COROT's 20 day programs and $v \cdot \sin i = 50\,{\rm km.s}^{-1}$ for COROT's 150 day programs.

It is important to bear in mind that the domain of validity obtained for perturbative methods depends on the choice of rotational variable used in the development. In order to illustrate this, suppose we develop a frequency in terms of two different rotational parameters X and Y: $\omega = a_0 + a_1 X + a_2 X^2 + a_3 X^3 + \mathcal{O}(X^4) = b_0 + b_1 Y + a_2 Y^2 + a_3 Y^3 + \mathcal{O}(Y^4)$. When the relationship between X and Y is more complex than a simple proportionality, the neglected terms, $\mathcal{O}(X^4)$ and $\mathcal{O}(Y^4)$, are not the same. As a result, a $3^{\rm rd}$ order development in terms of X or Y will give different values for ω, thus modifying the corresponding domain of validity. Therefore, we decided to compute the domain of validity associated with the variables Ω/Ω_K and $\Omega/(GM/R_{\rm pol}^3)^{1/2}$ to see if there was a substantial difference between the two. For individual frequencies, there can be large differences, but when all the frequencies are considered, the global result is roughly the same.

In Fig. 5, we show the differences between complete frequencies and perturbative ones at $0.59\Omega_K$. We have kept the same parameters for the equilibrium model as in Fig. 4. As can be seen from the figure, differences between the two sets of calculations are substantial and comparable to the large frequency separation (which seems to survive rotation). The order of frequencies is not the same between the two sets of calculations. As a result, it is necessary to use complete calculations in order to correctly interpret a pulsating star rotating at such a high rotation rate.

Recently, Suárez et al. (2005) attempted to model Altair through asteroseismology. The effects of rotation were included in the pulsation modes using $2^{\rm nd}$ order perturbative methods. Later interferometric studies suggested an equatorial velocity of $280\,{\rm km.s}^{-1}$ (Domiciano de Souza et al., 2005), which is above $216\,{\rm km.s}^{-1}$, the equatorial velocity corresponding to Fig. 5 (if we use a mass of $M = 1.8\,M_\odot$ and a polar radius $R_{\rm pol} = 1.7\,R_\odot$ instead, we obtain $v_{\rm eq} = 244\,{\rm km.s}^{-1}$). As a result, it is pretty obvious that what is required in Suárez et al. (2005) is complete calculations of the effects of rotation before being able to interpret Altair's oscillation spectrum (not to mention complete models of rapidly rotating stars).

4.1.3. Relative importance of the Coriolis and centrifugal forces

It is then interesting to analyse what is the main source of differences between perturbative calculations and complete ones. In Fig. 6 we show three different graphs which give the relative errors associated with different calculations:

$$\left(\frac{\delta\omega}{\omega}\right)_{(a)} = \frac{\omega_{\rm pert.} - \omega}{\omega}, \tag{68}$$

$$\left(\frac{\delta\omega}{\omega}\right)_{(b)} = \frac{\omega_{\rm pert.}^{\rm no\ Cor.} - \omega^{\rm no\ Cor.}}{\omega^{\rm no\ Cor.}}, \tag{69}$$

$$\left(\frac{\delta\omega}{\omega}\right)_{(c)} = \frac{\omega^{\rm no\ Cor.} - \omega}{\omega}, \tag{70}$$

where the subscripts (a), (b) and (c) correspond to the different panels in Fig. 6, the subscript "pert." to $3^{\rm rd}$ order perturbative calculations and the superscript "no Cor." to calculations done without the Coriolis force. From these panels, it is possible to deduce the dominant role of the centrifugal force in the differences between perturbative and complete calculations. Panels (a) and (b) are very similar, yet the first one includes the Coriolis force and the second one excludes it. Panel (c) shows the errors which come from excluding the Coriolis force. These errors are at least ten times smaller than in cases (a) and (b) and decrease with the radial order. This decrease is expected because as the
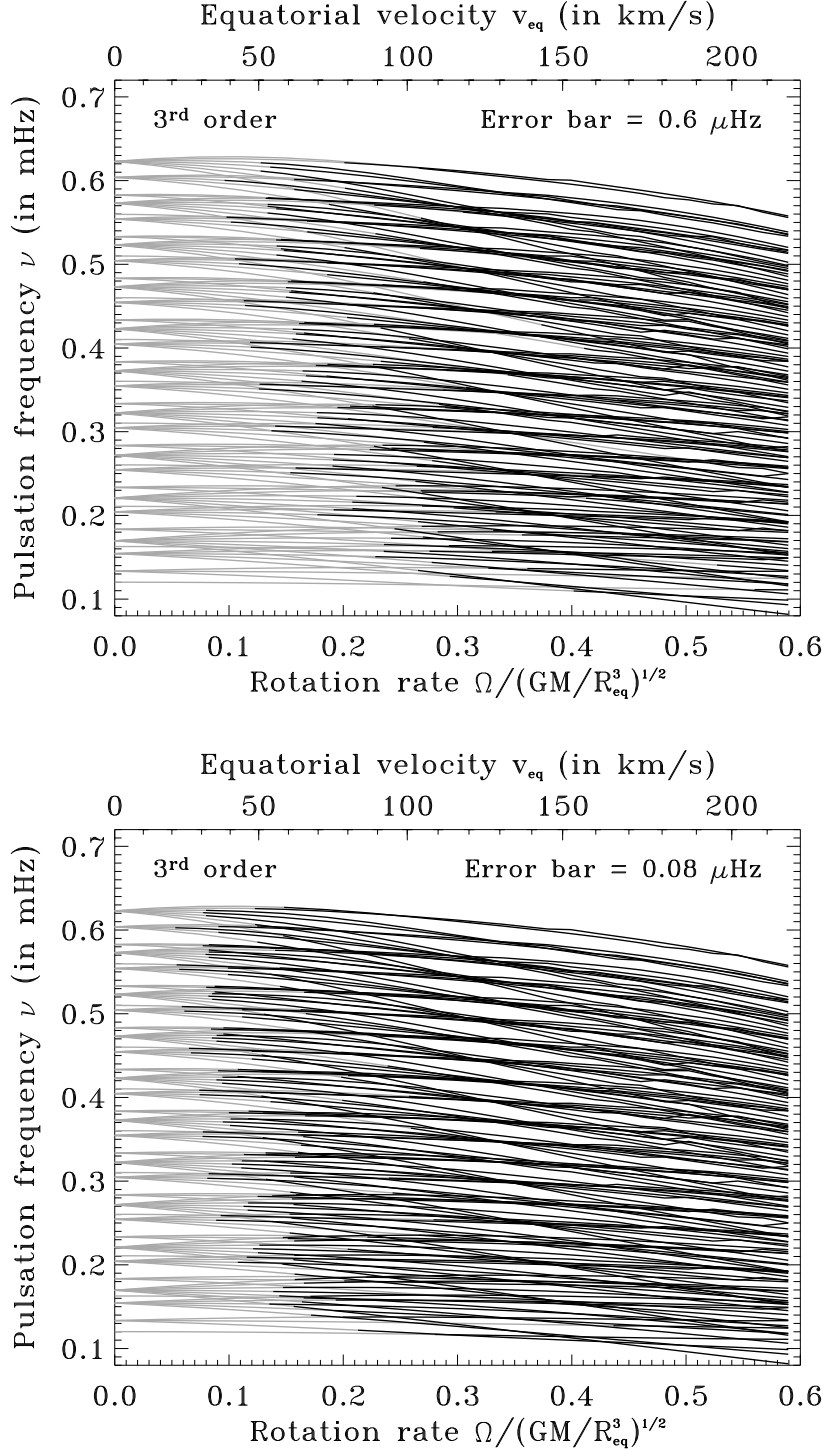
Figure 4. Plots of the evolution of pulsation cyclic frequencies ($\nu = \omega/2\pi$) as a function of the rotation rate. The frequencies are followed from the non-rotating case to $0.59\,\Omega_K$ using the procedure described in Paper I. At small rotation rates, it is easy to recognise the usual multiplet structure as predicted from perturbative methods. Once the rotation rate is sufficient large, the multiplets are less regular and overlap, which greatly complicates the interpretation of the oscillation spectrum. Superimposed is the domain of validity of $3^{\rm rd}$ order perturbative methods using COROT's error bars of $0.6\,\mu$Hz (upper panel) and $0.08\,\mu$Hz (lower panel). The calculations were done with $N = 3$ polytropic models with $R_{\rm pol} = 2.3R_\odot$ and $M = 1.9M_\odot$.

radial order n of the mode increases, the time scale of the oscillations decreases and becomes much shorter than the $1/\Omega$ time scale associated with the Coriolis force. As a result high order modes are less affected by the Coriolis force.

The effects of the centrifugal force, on the other hand, increase with radial order. The reason for this, as explained in Paper I, is that changes in the stellar structure and the sound velocity profile causes modifications which are roughly proportional to the frequencies. For spherically symmetric changes in a star's structure, we have $\Delta \ln \omega = -\Delta \ln \int_0^R dr/c$ (where Δ means the variations due to the change in stellar structure), based on Tassoul's asymptotic formula (Tassoul, 1980). The same principle applies for more complicated changes in the structure, such as those provoked by the centrifugal force, but will have a more complicated mathematical formulation. One way of illustrating this is by plotting the ratios D_1/ω_0 (see Eq. (66)), which correspond to $\partial \ln \omega/\partial\Omega^2$ calculated at $\Omega = 0$ for $m = 0$ modes. We take the derivative with respect to Ω^2 since the effects of the centrifugal force begin at $2^{\rm nd}$ order in Ω. In Fig. 7, we can see that these ratios approach constant values as n increases for a given ℓ. Furthermore, we have plotted these
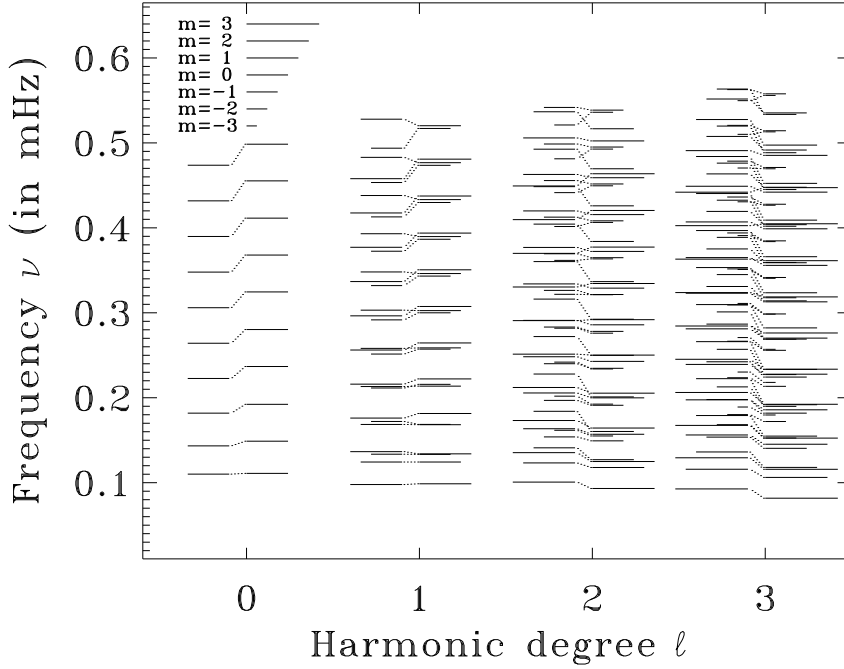
Figure 5. This figure shows a comparison between perturbative cyclic frequencies and complete ones at $0.59\Omega_K$. The equilibrium model is the same as in Fig. 4. The complete calculations are represented by the bars that go to the right and the perturbative ones by the bars going to the left. The length of the bars gives the azimuthal order. Complete and perturbative calculations are connected by dotted lines (the correspondence is based on mode labelling as described in Paper I). It is clear from this figure that perturbative calculations lead to substantial error at high rotation rates, and cannot correctly anticipate the order of the modes. Even if the perturbative frequencies were multiplied by a global corrective factor, the agreement remains poor.

ratios both with and without the Coriolis force, thereby demonstrating that this effect is entirely due to the centrifugal force. For non-axisymmetric modes, the relevant ratios $(D_1 + m^2 D_2)/\omega_0$ also show the same behaviour. This shows that the effects of the centrifugal distortion is roughly proportional to the frequency.

It can then be expected that making errors on the effects of the centrifugal force will also lead to differences proportional to the frequencies. If we look at panel (b) of Fig. 6 in which the Coriolis force has been suppressed, we can see that the relative differences between perturbative and complete calculations $\delta\omega/\omega$ actually increase with radial order (at least for lower and moderate rotation rates). It is an open question whether or not these relative differences will approach an asymptotic limit as the radial order increases like in Fig. 7.

The increase of perturbative errors with radial order may have important implications for stars which pulsate in high radial overtones. Examples of these are solar type stars which typically pulsate with radial orders between 15 and 25. If we assume that perturbative errors scale with frequency and frequency with radial order, we can estimate at what point complete methods will be necessary to calculate the effects of rotation on such modes. The average limit for $n = 25$ pulsation modes in $M = 1\,M_\odot$, $R_{\mathrm{pol}} = 1\,R_\odot$ stars would be $v_{\mathrm{eq}} = 25\,\mathrm{km.s}^{-1}$ ($45\,\mathrm{km.s}^{-1}$) for COROT's primary (secondary, resp.) program. This implies that non-perturbative effects of rotation could be visible for moderate rotation rates. Nonetheless, direct comparisons between perturbative and complete calculations for high order modes are necessary to confirm this conclusion.

In order to further understand the role of the centrifugal force in perturbative errors, it is helpful to bear in mind the approximations which result from applying perturbative methods. First of all, the frequencies, the stellar structure and the mode structure are all described by low degree polynomials in Ω. This then leads to the following effects: the equilibrium structure is only described by $\ell = 0$ and $\ell = 2$ spherical harmonics (for 2nd and 3rd order methods) and the pulsation mode structure is also limited to a few spherical harmonics. In order to analyse the effects of using only a few spherical, we did highly truncated numerical calculations, in which the equilibrium model has been reduced to 2 spherical harmonics and the pulsation modes to 4 spherical harmonics (2 poloidal + 2 toroidal). In Fig. 8, the black lines represent the relative differences between these truncated calculations and complete ones. These differences are significant, thus showing the need for more spherical harmonics. Nonetheless, we also plot in Fig. 8 the perturbative errors which are higher than the truncated calculations. This shows that including higher order terms in Ω in the contribution of even the lowest degree spherical harmonics can improve results.

4.2. Discussion

As can be seen from previous sections, differences between perturbative calculations and complete ones can be quite substantial. This is problematic because obtaining accurate results is crucial in asteroseismology. Differences between theoretical calculations and observed frequencies need to come from differences between the stellar model and the star's actual structure rather than from an approximate treatment of the effects of rotation. Otherwise, modifying the stellar structure so as to match the observed frequencies will end up compensating errors in the calculation
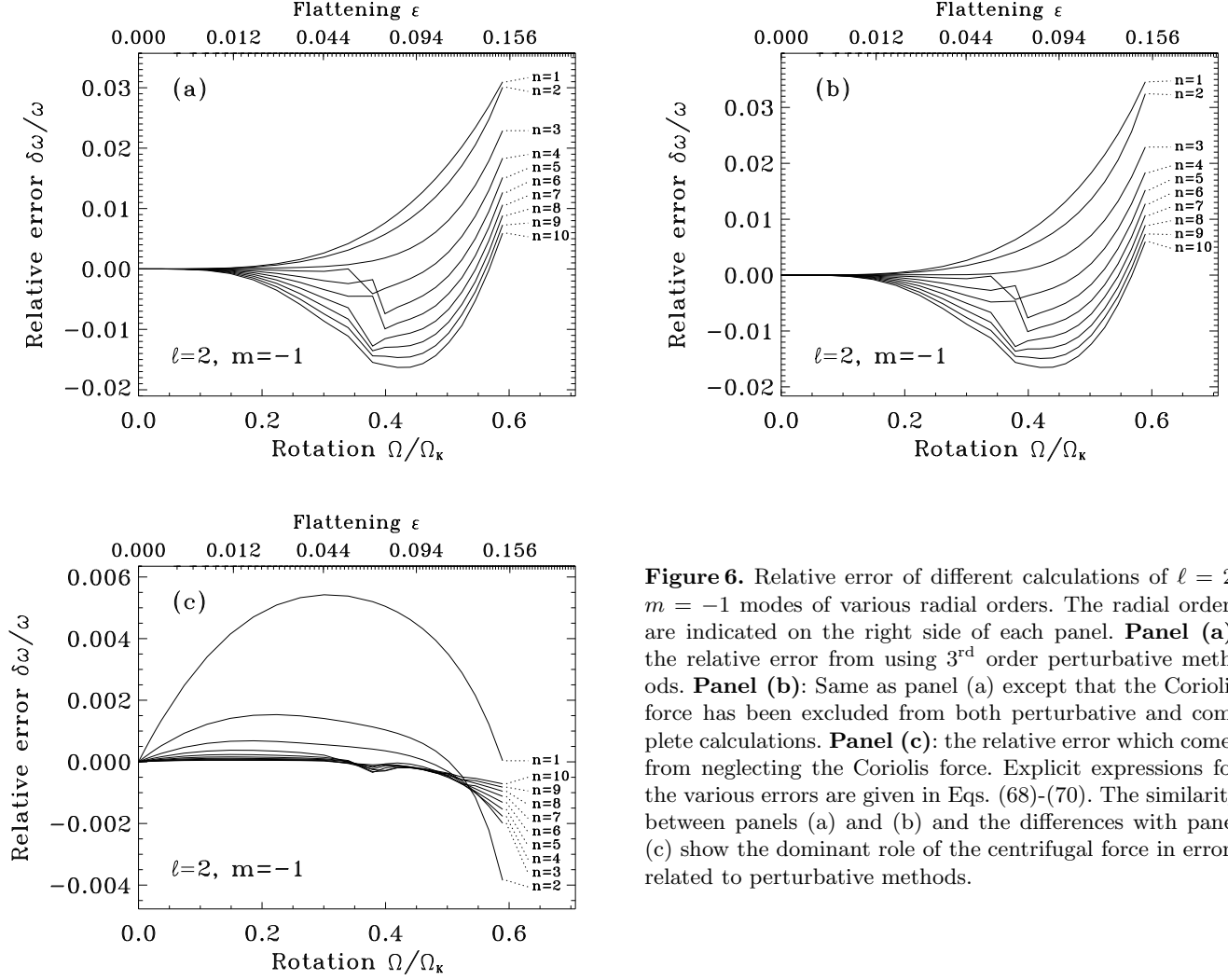
Figure 6. Relative error of different calculations of $\ell = 2$, $m = -1$ modes of various radial orders. The radial orders are indicated on the right side of each panel. **Panel (a)**: the relative error from using 3rd order perturbative methods. **Panel (b)**: Same as panel (a) except that the Coriolis force has been excluded from both perturbative and complete calculations. **Panel (c)**: the relative error which comes from neglecting the Coriolis force. Explicit expressions for the various errors are given in Eqs. (68)-(70). The similarity between panels (a) and (b) and the differences with panel (c) show the dominant role of the centrifugal force in errors related to perturbative methods.

of frequencies instead of improving the stellar model. Moreover, large errors on frequency calculations can lead to erroneous mode identifications, especially if proximity between observed and theoretical frequencies is the only criteria used for establishing such identifications. Interestingly, establishing a correct mode identification is one of the key difficulties in interpreting δ Scuti stars (*e.g.* Goupil et al., 2005). Mode misidentification can occur because frequencies are not in the same order in perturbative calculations as in complete ones (in Fig. 5, this can be seen by the dotted lines for the $\ell = 1$, 2 or 3 modes which cross each other, thus indicating an exchange of position between two frequencies) and because one can no longer rely on the usual frequency patterns used in slowly rotating stars (see Paper I). An erroneous mode identification then leads a false interpretation of pulsation frequencies due to an incorrect understanding of the geometry of the pulsation mode and the stellar regions which it probes. This problem is further aggravated by the fact that perturbative methods only give an approximate idea of the structure of a given mode anyway. Fully taking into account the effects of rotation on stellar pulsation increases the likelihood of obtaining a correct identification and gives a better understanding of mode structure, especially when the rotation rate is high. However, in order to obtain such a mode identification, the underlying stellar model needs to be sufficiently close to reality so as enable a successful matching between theoretical predictions and observations. It is possible that even then, mode identification is uncertain due to multiple solutions which fit a set of observed frequencies.

5. Conclusion

In this work we have explored some of the effects of rapid rotation on stellar acoustic pulsations. This was achieved thanks to a numerical method which combines spheroidal geometry and spectral methods, as in Paper I. Through a detailed analysis, we have shown that our results have a 6 to 7 digit accuracy. This analysis included a discussion on the accuracy of the underlying polytropic models, comparisons with Saio (1981), Clement (1984), Christensen-Dalsgaard
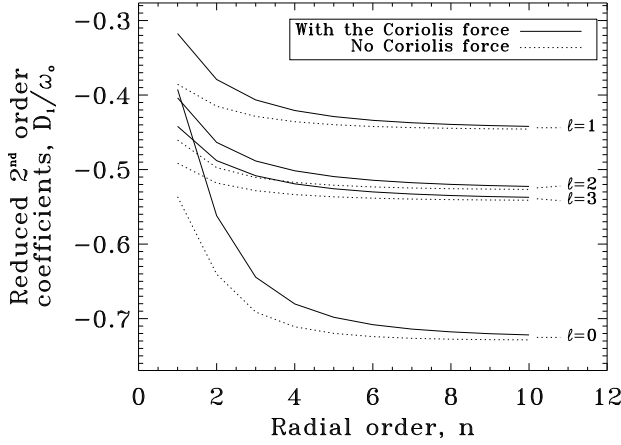
Figure 7. Ratio of 2nd order perturbative coefficients to corresponding frequencies at $\Omega = 0$, as a function of the radial order n. As n increases, these ratios approach a constant value, which shows the proportional effects of the centrifugal deformation of the star.
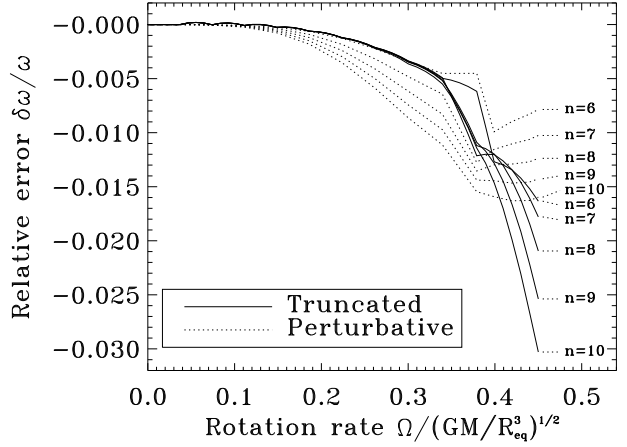
Figure 8. A comparison between relative errors in perturbative calculations and those in truncated calculations (in which the equilibrium model is reduced to 2 spherical harmonics and the pulsation mode to 2 poloidal + 2 toroidal harmonics). This figure shows that truncated calculations are closer to complete ones than perturbative calculations, which shows the importance of retaining higher powers of Ω in the lower spherical harmonics describing the stellar structure and mode structure. The uneven aspect of the lines corresponding to the truncated calculations are due to interpolation errors.

& Mullan (1994) and Paper I, a test based on the variational principle and some tests on the sensitivity of the results to the parameters of the numerical method.

In the future, the satellite COROT is expected to measure stellar oscillation frequencies with a precision of $0.08\,\mu$Hz (primary targets) or $0.6\,\mu$Hz (secondary targets). In the frequency range considered in this paper, we find that for a $M = 1.9\,M_\odot$, $R = 2.3\,R_\odot$ star, perturbative methods cease to be valid for COROT's primary (secondary) program beyond $v \cdot \sin i = 50\,\text{km.s}^{-1}$ ($v \cdot \sin i = 75\,\text{km.s}^{-1}$, resp.). At a rotation rate of $0.59\,\Omega_K$, the perturbative spectrum is very different from the one based on complete calculations. Therefore, any attempt to interpret stellar pulsations using the perturbative approach at comparable rotation rates is likely to fail. Using complete methods on the other hand increases the likelihood of obtaining a correct mode identification, and gives an accurate description of the structure of pulsation modes. Both of these are crucial when interpreting observed pulsation modes.

Further investigation has shown the dominant role of the centrifugal force in modifying the frequency spectrum and causing perturbative errors. This is because while the effect of the Coriolis force decreases as the frequency increases, the effect of the stellar deformation increases roughly proportionally to the frequencies. Therefore, the errors which arise from perturbative descriptions of the centrifugal distortion are also amplified in higher order modes. As a result, it may be necessary to use complete methods for moderately rotating stars which exhibit high order modes.

Some of the issues which were discussed in Paper I and have yet to be discussed for the present results include: an analysis of the regularities in the oscillation spectrum at high rotation rates and a study of the visibility of the different modes based on their structure. These will be the subject of forthcoming papers. A few preliminary examinations have already confirmed some of the conclusions given in Paper I, such as a strong equatorial concentration of mode structure at high rotation rates, or the transition from one frequency spectrum organisation to another.

Future work includes working with more realistic models, and studying gravity modes in spheroidal geometry. The transition to more realistic models is essential before being able to compare theoretical frequencies with observations. Coming up with realistic models that fully include the effects of rotation and in particular the centrifugal distortion is no easy task, but is the subject of active research (*e.g.* Roxburgh, 2004, Jackson et al., 2005, Rieutord et al., 2005). Calculating the associated pulsation frequencies and comparing them to observations will provide crucial information on stellar structure and enable a better adjustment of these models.

The study of the effects of rapid rotation on g-modes is of interest for the interpretation of γ Doradus stars, which are g-mode pulsators and can be rapid rotators. Previous studies on the non-perturbative effects of the Coriolis force on g-modes (Dintrans et al., 1999, Dintrans & Rieutord, 2000) have revealed their important role in altering the geometry and frequencies of these modes. This behaviour is entirely different from that of the high frequency acoustic

modes presented here. It is then interesting to understand what the effects of the centrifugal force will be on g-modes and how it will compare with the effects of the Coriolis force.

References

Baglin, A., Auvergne, M., Barge, P., et al. 2002, in ESA SP-485: Stellar Structure and Habitable Planet Finding, ed. B. Battrick, F. Favata, I. W. Roxburgh, & D. Galadi, 17–24

Bender, C. M. & Orszag, S. A. 1978, Advanced Mathematical Methods for Scientists and Engineers (McGraw-Hill)

Bonazzola, S., Gourgoulhon, E., & Marck, J.-A. 1998, Phys. Rev. D, 58, 104020

Canuto, C., Hussaini, M. Y., Quarteroni, A., & Zang, T. A. 1988, Spectral Methods in Fluid Dynamics (Springer Verlag)

Chatelin, F. 1988, Valeurs propres de matrices (Paris: Masson)

Christensen-Dalsgaard, J. & Mullan, D. J. 1994, MNRAS, 270, 921

Clement, M. J. 1981, ApJ, 249, 746

—. 1984, ApJ, 276, 724

—. 1986, ApJ, 301, 185

—. 1989, ApJ, 339, 1022

—. 1998, ApJS, 116, 57

Dintrans, B. & Rieutord, M. 2000, A&A, 354, 86

Dintrans, B., Rieutord, M., & Valdettaro, L. 1999, Journal of Fluid Mechanics, 398, 271

Domiciano de Souza, A., Kervella, P., Jankov, S., et al. 2003, A&A, 407, L47

—. 2005, A&A, 442, 567

Dziembowski, W. A. & Goode, P. R. 1992, ApJ, 394, 670

Espinosa, F., Pérez Hernández, F., & Roca Cortés, T. 2004, in ESA SP-559: SOHO 14 Helio- and Asteroseismology: Towards a Golden Future, 424–427

Gough, D. O. & Thompson, M. J. 1990, MNRAS, 242, 25

Goupil, M.-J., Dupret, M. A., Samadi, R., et al. 2005, JA&A, 26, 249

Hachisu, I., Eriguchi, Y., & Sugimoto, D. 1982, Progress of Theoretical Physics, 68, 191

Hunter, C. 2001, MNRAS, 328, 839

Hurley, M., Roberts, P. H., & Wright, K. 1966, ApJ, 143, 535

Ipser, J. & Lindblom, L. 1990, ApJ, 355, 226

Jackson, S., MacGregor, K. B., & Skumanich, A. 2005, ApJS, 156, 245

Karami, K., Christensen-Dalsgaard, J., Pijpers, F. P., Goupil, M. ., & Dziembowski, W. A. 2005, [arXiv: astroph/0502194]

Ledoux, P. 1951, ApJ, 114, 373

Lignières, F., Rieutord, M., & Reese, D. 2006a, A&A, 455, 607, (Paper I)

—. 2006b, Memorie della Societa Astronomica Italiana, 77, 425

Lynden-Bell, D. & Ostriker, J. P. 1967, MNRAS, 136, 293

Peterson, D. M., Hummel, C. A., Pauls, T. A., et al. 2006, ApJ, 636, 1087

Rieutord, M. 1987, Geophys. Astrophys. Fluid Dynamics, 39, 163

—. 2006, A&A, 451, 1025

Rieutord, M., Dintrans, B., Lignières, F., Corbard, T., & Pichon, B. 2005, in SF2A-2005: Semaine de l'Astrophysique Francaise, 759

Rieutord, M. & Valdettaro, L. 1997, Journal of Fluid Mechanics, 341, 77

Roxburgh, I. W. 2004, A&A, 428, 171

Saio, H. 1981, ApJ, 244, 299

Seidov, Z. F. 2004, [arXiv: astroph/0402130]

Soufi, F., Goupil, M.-J., & Dziembowski, W. A. 1998, A&A, 334, 911

Suárez, J. C., Bruntt, H., & Buzasi, D. 2005, A&A, 438, 633

Tassoul, M. 1980, ApJS, 43, 469

Unno, W., Osaki, Y., Ando, H., Saio, H., & Shibahashi, H. 1989, Nonradial oscillations of stars, 2nd edn. (University of Tokyo Press)

Valdettaro, L., Rieutord, M., Braconnier, T., & Fraysyé, V. 2006, Journal of Computational and Applied Mathematics, in press, [arXiv: physics/0604219]

Yoshida, S. & Eriguchi, Y. 1995, ApJ, 438, 830
—. 2001, MNRAS, 322, 389

Appendix A: "Generalised" Frobenius method

A.1. Description

The starting point in this method is the following equation:

$$\frac{dY(x,y,z)}{dx} + \frac{1}{x}A(x,y,z)Y(x,y,z) = 0. \tag{A.1}$$

This equation looks very much like a first order Frobenius equation except that two other variables, y and z, intervene in the different terms (for a description of the more traditional version of the Frobenius method, see Bender & Orszag, 1978). The quantity $Y(x,y,z)$ can be a scalar or a vector. The operator $A(x,y,z)$ can include derivatives in the y and z directions and needs to be analytic in the x direction, so that we can write:

$$A(x,y,z) = \sum_{n=0}^{\infty} A_n(y,z)x^n. \tag{A.2}$$

We then look for the behaviour of $Y(x,y,z)$ along the boundary $x = 0$. If we develop $Y(x,y,z)$ in the following manner,

$$Y(x,y,z) = \sum_{n=0}^{\infty} Y_n(y,z)x^{n+\alpha}, \tag{A.3}$$

then we obtain the following zeroth order equation:

$$\alpha Y_0(y,z) + A_0(y,z)Y_0(y,z) = 0, \tag{A.4}$$

where α is the leading power of x in $Y(x,y,z)$. Therefore, to obtain α, one needs to solve an eigenvalue problem in terms of the coordinates y and z, along the entire surface $x = 0$. The remaining Y_n are defined through the following recurrence relation:

$$n \geq 1, \quad [(\alpha + n)Id + A_0]Y_n = -\sum_{k=0}^{n-1} A_{n-k}Y_k, \tag{A.5}$$

where $Id(Y) \equiv Y$. This series is defined only if for each $n \geq 1$, the operator $[(\alpha + n)Id + A_0]$ is invertible. The next step is then to search under what mathematical conditions the series defined by Eq. (A.5) converges. However, this step is quite complicated and therefore beyond the scope of this paper.

A.2. Application

In our case, we are only interested in obtaining the leading behaviour of our solutions near the surface. Therefore we will only solve the zeroth order equation (Eq. (A.4)) after having established the expressions for Y_0 and A_0. We start by defining $x = 1 - \zeta$ as the variable that will be used in the Frobenius series. The surface of the star then corresponds to $x = 0$ and its interior to positive values of x.

It is then necessary to choose a vector Y so that Eqs. (33)-(38) can be put in the form given by Eq. (A.1). This implies choosing the variables which are differentiated once with respect to x. Our choice is therefore $Y = [\Pi, u^\zeta, \mathcal{G} = \partial_x\Psi, \Psi]^t$. Having chosen the vector Y, it is then necessary to find the associated system of equations, by eliminating the variables (b, u^θ, u^ϕ), and then to extract the zeroth order equation (see Eq. (A.4)). In fact, it is much simpler to do both steps simultaneously, given the complexity of Eqs. (33)-(38).

Before giving the final result, it is important to point out that when N is not an integer, a mild singularity occurs on the surface of the star, due to the presence of fractional powers in the enthalpy, starting with x^{N+2} (Hunter, 2001). This in fact invalidates the use of Frobenius series in its present form from a strictly mathematical point of view, since these only use integer powers of x. This problem can be solved by including fractional powers in the solution, as is done in Christensen-Dalsgaard & Mullan (1994), the lowest one being x^{N+1} (this is not in contradiction with Christensen-Dalsgaard & Mullan (1994), for which the variable y_4 contains x^N, because y_4 includes $\partial_{xx}H$ in its expression whereas

our variables do not). As a result, the zeroth order equation remains unaffected and can therefore give the correct behaviour of the solution near the surface:

$$
\alpha
\begin{bmatrix}
\Pi_0 \\
u_0^\zeta \\
\mathcal{G}_0 \\
\Psi_0
\end{bmatrix}
+
\begin{bmatrix}
N\left(1-\dfrac{\gamma}{\Gamma_1}\right) & \dfrac{NH_x}{\lambda\Lambda(1-\varepsilon)R_s^2}\left(\dfrac{\gamma}{\Gamma_1}-1\right) & 0 & 0 \\
-\dfrac{\lambda\Lambda(1+N)(1-\varepsilon)R_s^2}{H_x\Gamma_1} & \dfrac{1+N}{\Gamma_1} & 0 & 0 \\
0 & 0 & 0 & 0 \\
0 & 0 & 0 & 0
\end{bmatrix}
\begin{bmatrix}
\Pi_0 \\
u_0^\zeta \\
\mathcal{G}_0 \\
\Psi_0
\end{bmatrix}
= 0.
\tag{A.6}
$$

This equation is based on the following development of the enthalpy near the surface:

$$
H(x,\theta) = H_x(\theta)x + \frac{1}{2}H_{xx}(\theta)x^2 + H_N(\theta)x^{N+2} + o(x^2).
\tag{A.7}
$$

The characteristic equation is $det(A_0 - X.Id) = X^4 - NX^3 = 0$. The eigenvalues are therefore $\alpha = -N$ and $\alpha = 0$, the second value being triply degenerate. The first value is rejected because it leads to solutions that diverge on the surface of the star. The three remaining eigensolutions are bounded near the surface, which is in complete agreement with the results of Hurley et al. (1966), who applied the Frobenius method to the spherical case. By choosing $\alpha = 0$, we also ensure that $[(\alpha + n)Id + A_0]$ is invertible for $n \geq 1$. These three bounded solutions and any of their linear combinations satisfy the following analytical constraint:

$$
\lambda\Pi_0 = \frac{H_x}{\Lambda(1-\varepsilon)R_s^2}u_0^\zeta,
\tag{A.8}
$$

which is, in fact, equivalent to saying that $\delta p/\rho_0$ goes to zero on the outer boundary (where δp represents the Lagrangian variation of the pressure). We can use the previous results to establish the behaviour of different quantities near the surface:

$$
\begin{aligned}
p &= \mathcal{O}\left(x^N\right), & \text{(A.9)} \\
\rho &= \mathcal{O}\left(x^{N-1}\right), & \text{(A.10)} \\
u^\zeta &= \mathcal{O}(1), & \text{(A.11)} \\
u^\theta &= \mathcal{O}(1), & \text{(A.12)} \\
u^\phi &= \mathcal{O}(1), & \text{(A.13)} \\
\Psi &= \mathcal{O}(1). & \text{(A.14)}
\end{aligned}
$$

Eq. (A.8) shows that $\delta p/H^N = o(1)$. The next relevant power in a power series expansion of $\delta p/H^N$ is x^1 (this remains true even when N is not an integer since the first fractional power of $\delta p/H^N$ is $N+1$). By applying the equation $\delta p = c_o^2\delta\rho$, it can also be shown that $\delta\rho/H^{N-1} = \mathcal{O}(x)$. As a result we obtain the following behaviour for both Lagrangian perturbations:

$$
\begin{aligned}
\delta p &= \mathcal{O}\left(x^{N+1}\right), & \text{(A.15)} \\
\delta\rho &= \mathcal{O}\left(x^N\right). & \text{(A.16)}
\end{aligned}
$$

The results on ρ, p, $\delta\rho$, δp are interesting when we consider the equilibrium model. Since $\rho_o \propto H^N$ and $P_o \propto H^{N+1}$, we deduce that the leading behaviour of the equilibrium density and pressure are $\rho_o = \mathcal{O}\left(x^N\right)$ and $P_o = \mathcal{O}\left(x^{N+1}\right)$, respectively. This implies that the ratio of the Eulerian density perturbation to the equilibrium density (ρ/ρ_o) and the corresponding ratio for pressure both become unbounded as one approaches the surface of the star. This is problematic because the sum $\rho_o + A\,\rho\,\cos(\omega t)$ (which corresponds to the total density) will periodically reach negative values close to the surface of the star for any non-zero amplitude A. However, the ratio of the Lagrangian density perturbation to the equilibrium density remains bounded as one approaches the surface, and the same applies to the pressure. This suggests that a Lagrangian description is physically more appropriate.

Appendix B: Projection onto the spherical harmonic base

B.1. Integral operators

In order to project the fluid equations onto the harmonic basis, it is necessary to define a number of integral operators. The prototype to one of these operators is as follows:

$$
J_{\ell\ell'}^m(G)(\zeta) = \iint_{4\pi} G(\zeta,\theta)\partial_\theta Y_{\ell'}^m(\theta,\phi)\left\{Y_\ell^m(\theta,\phi)\right\}^* \mathrm{d}\Omega,
\tag{B.1}
$$

where $d\Omega = \sin\theta d\theta d\phi$, G is an arbitrary function, x^* is the complex conjugate of x and $J_{\ell\ell'}^m(.)$ is the operator. $J_{\ell\ell'}^m(G)$ is a two-dimension array of indexes ℓ and ℓ' (the value of m is fixed) composed of functions depending on ζ only. The remaining operators are given in the following table:

	$\{Y_\ell^m\}^*$	$\{\partial_\theta Y_\ell^m\}^*$	$\{\mathrm{D}_\phi Y_\ell^m\}^*$
$Y_{\ell'}^m$	$I_{\ell\ell'}^m(G)$	$Jc_{\ell\ell'}^m(G)$	$Kc_{\ell\ell'}^m(G)$
$\partial_\theta Y_{\ell'}^m$	$J_{\ell\ell'}^m(G)$	$L_{\ell\ell'}^m(G)$	$Mc_{\ell\ell'}^m(G)$
$\mathrm{D}_\phi Y_{\ell'}^m$	$K_{\ell\ell'}^m(G)$	$M_{\ell\ell'}^m(G)$	$N_{\ell\ell'}^m(G)$

If G is a real function than $I_{\ell\ell'}^m(G)$, $J_{\ell\ell'}^m(G)$, $Jc_{\ell\ell'}^m(G)$, $L_{\ell\ell'}^m(G)$ and $N_{\ell\ell'}^m(G)$ are all real functions whereas $K_{\ell\ell'}^m(G)$, $Kc_{\ell\ell'}^m(G)$, $M_{\ell\ell'}^m(G)$, and $Mc_{\ell\ell'}^m(G)$ are purely imaginary. There are symmetries between some of these operators: for example $J_{\ell\ell'}^m(G^*) = \{Jc_{\ell'\ell}^m(G)\}^*$. The same applies for $K_{\ell\ell'}^m(G)$ and $Kc_{\ell\ell'}^m(G)$, and for $M_{\ell\ell'}^m(G)$ and $Mc_{\ell\ell'}^m(G)$.

In order to calculate these integrals, we use Gauss' quadrature. This gives accurate integrals when G is a "polynomial" of $\cos\theta$ (the coefficients of the polynomial can depend on ζ), for the operators $I_{\ell\ell'}^m(G)$, $L_{\ell\ell'}^m(G)$, $M_{\ell\ell'}^m(G)$, $Mc_{\ell\ell'}^m(G)$ and $N_{\ell\ell'}^m(G)$. For the operators $J_{\ell\ell'}^m(G)$, $K_{\ell\ell'}^m(G)$, $Jc_{\ell\ell'}^m(G)$ and $Kc_{\ell\ell'}^m(G)$, G needs to be of the form $\sin\theta P(\cos\theta)$ where P is a polynomial. These integrals are calculated with L_{res} collocation points, where L_{res} is generally greater than L_{max}, the harmonic resolution of the pulsations.

Having defined the different integral operators, it is now possible to give explicitly the fluid equations projected onto the spherical harmonic basis. In what follows, we have used the following conventions:

$$I_{\ell\ell'}^m(G)\, u_m^{\ell'} \equiv \sum_{\ell'} I_{\ell\ell'}^m(G)\, u_m^{\ell'}, \qquad \begin{matrix} -L_{\ell\ell'}^m \\ +N_{\ell\ell'}^m \end{matrix}(G) \equiv -L_{\ell\ell'}^m(G) + N_{\ell\ell'}^m(G). \tag{B.2}$$

It is also worth pointing out that in the following matrices, the summation on ℓ' applies to an entire line of the matrix. For example,

$$\begin{bmatrix} +I_{\ell\ell'}^m(A) - J_{\ell\ell'}^m(B) & u_m^{\ell'} \\ -K_{\ell\ell'}^m(C) + N_{\ell\ell'}^m(D) & v_m^{\ell'} \end{bmatrix}, \tag{B.3}$$

is equivalent to:

$$\sum_{\ell'=|m|}^{L} \{I_{\ell\ell'}^m(A) - J_{\ell\ell'}^m(B)\}\, u_m^{\ell'} + \sum_{\ell'=|m|}^{L} \{-K_{\ell\ell'}^m(C) + N_{\ell\ell'}^m(D)\}\, v_m^{\ell'}. \tag{B.4}$$

B.2. Continuity equation

$$\lambda b_m^\ell = \begin{bmatrix} -I_{\ell\ell'}^m\left(\dfrac{\zeta^2 H}{r^2 r_\zeta}\right) & \partial_\zeta u_m^{\ell'} \\[2ex] -I_{\ell\ell'}^m\left(\dfrac{2\zeta H}{r^2 r_\zeta} + \dfrac{\zeta^2 N H_\zeta}{r^2 r_\zeta}\right) & u_m^{\ell'} \\[2ex] +I_{\ell\ell'}^m\left(\dfrac{\ell'(\ell'+1)\zeta H}{r^2 r_\zeta}\right) - J_{\ell\ell'}^m\left(\dfrac{\zeta N H_\theta}{r^2 r_\zeta}\right) & v_m^{\ell'} \\[2ex] -K_{\ell\ell'}^m\left(\dfrac{\zeta N H_\theta}{r^2 r_\zeta}\right) & w_m^{\ell'} \end{bmatrix}, \tag{B.5}$$

where we have made use of the following identities:

$$-\ell(\ell+1)Y_\ell^m = \partial_{\theta\theta}^2 Y_\ell^m + \cot\theta\,\partial_\theta Y_\ell^m + \frac{1}{\sin^2\theta}\partial_{\phi\phi}^2 Y_\ell^m, \tag{B.6}$$

$$0 = \partial_\theta \mathrm{D}_\phi Y_\ell^m + \cot\theta\,\mathrm{D}_\phi Y_\ell^m - \frac{1}{\sin\theta}\partial_\phi\partial_\theta Y_\ell^m. \tag{B.7}$$

B.3. Adiabatic energy equation

$$\lambda\left(\Pi_m^\ell - \frac{\Gamma_1}{(N+1)\Lambda}b_m^\ell\right) = \left(\frac{\Gamma_1}{\gamma} - 1\right)\begin{bmatrix} +I_{\ell\ell'}^m\left(\dfrac{\zeta^2 H_\zeta}{\Lambda r^2 r_\zeta}\right) & u_m^{\ell'} \\[2ex] +J_{\ell\ell'}^m\left(\dfrac{\zeta H_\theta}{\Lambda r^2 r_\zeta}\right) & v_m^{\ell'} \\[2ex] +K_{\ell\ell'}^m\left(\dfrac{\zeta H_\theta}{\Lambda r^2 r_\zeta}\right) & w_m^{\ell'} \end{bmatrix}. \tag{B.8}$$

B.4. Poisson's equation

$$
0 = \begin{bmatrix}
+I_{\ell\ell'}^m \left(\dfrac{r^2 + r_\theta^2}{r_\zeta^2} \right) & \partial_{\zeta\zeta}^2 \Psi_m^{\ell'} \\[2ex]
+I_{\ell\ell'}^m \left(r^2 c_\zeta \right) - 2J_{\ell\ell'}^m \left(\dfrac{r_\theta}{r_\zeta} \right) & \partial_\zeta \Psi_m^{\ell'} \\[2ex]
-\ell(\ell+1) & \Psi_m^{\ell} \\[1ex]
-I_{\ell\ell'}^m \left(r^2 H^{N-1} \right) & b_m^{\ell'}
\end{bmatrix},
\tag{B.9}
$$

where we have made use of the Eq. (B.6).

B.5. Euler's equations

$$
\lambda \begin{bmatrix}
+I_{\ell\ell'}^m \left(\dfrac{\zeta^2 r_\zeta H}{r^2} \right) & u_m^{\ell'} \\[2ex]
+J_{\ell\ell'}^m \left(\dfrac{\zeta r_\theta H}{r^2} \right) & v_m^{\ell'} \\[2ex]
+K_{\ell\ell'}^m \left(\dfrac{\zeta r_\theta H}{r^2} \right) & w_m^{\ell'}
\end{bmatrix} =
\begin{bmatrix}
+K_{\ell\ell'}^m \left(\dfrac{2\Omega H \zeta \sin\theta}{r} \right) & v_m^{\ell'} \\[2ex]
-J_{\ell\ell'}^m \left(\dfrac{2\Omega H \zeta \sin\theta}{r} \right) & w_m^{\ell'} \\[2ex]
-I_{\ell\ell'}^m \left(H \right) & \partial_\zeta \Pi_m^{\ell'} \\[1ex]
-I_{\ell\ell'}^m \left(H \right) & \partial_\zeta \Psi_m^{\ell'} \\[1ex]
-I_{\ell\ell'}^m \left(N H_\zeta \right) & \Pi_m^{\ell'} \\[1ex]
+I_{\ell\ell'}^m \left(\dfrac{H_\zeta}{\Lambda} \right) & b_m^{\ell'}
\end{bmatrix},
\tag{B.10}
$$

$$
\lambda \begin{bmatrix}
+Jc_{\ell\ell'}^m \left(\dfrac{\zeta r_\theta}{r^2} \right) & u_m^{\ell'} \\[2ex]
+L_{\ell\ell'}^m \left(\dfrac{r^2 + r_\theta^2}{r^2 r_\zeta} \right) + N_{\ell\ell'}^m \left(\dfrac{1}{r_\zeta} \right) & v_m^{\ell'} \\[2ex]
+M_{\ell\ell'}^m \left(\dfrac{r^2 + r_\theta^2}{r^2 r_\zeta} \right) - Mc_{\ell\ell'}^m \left(\dfrac{1}{r_\zeta} \right) & w_m^{\ell'}
\end{bmatrix} =
\begin{bmatrix}
-Kc_{\ell\ell'}^m \left(\dfrac{2\Omega \zeta \sin\theta}{r} \right) & u_m^{\ell'} \\[2ex]
+M_{\ell\ell'}^m \left(\dfrac{2\Omega(r_\theta \sin\theta + r\cos\theta)}{rr_\zeta} \right) & v_m^{\ell'} \\
-Mc_{\ell\ell'}^m & \\[1ex]
-L_{\ell\ell'}^m \left(\dfrac{2\Omega(r_\theta \sin\theta + r\cos\theta)}{rr_\zeta} \right) & w_m^{\ell'} \\
-N_{\ell\ell'}^m & \\[1ex]
-L_{\ell\ell'}^m \left(\dfrac{1}{\zeta} \right) - Jc_{\ell\ell'}^m \left(\dfrac{NH_\theta}{\zeta H} \right) & \Pi_m^{\ell'} \\
-N_{\ell\ell'}^m \left(\dfrac{1}{\zeta} \right) & \\[1ex]
-L_{\ell\ell'}^m \left(\dfrac{1}{\zeta} \right) & \Psi_m^{\ell'} \\
-N_{\ell\ell'}^m \left(\dfrac{1}{\zeta} \right) & \\[1ex]
+Jc_{\ell\ell'}^m \left(\dfrac{H_\theta}{\Lambda \zeta H} \right) & b_m^{\ell'}
\end{bmatrix},
\tag{B.11}
$$

$$
\lambda \begin{bmatrix}
+Kc_{\ell\ell'}^m \left(\dfrac{\zeta r_\theta}{r^2} \right) & u_m^{\ell'} \\[2ex]
+Mc_{\ell\ell'}^m \left(\dfrac{r^2 + r_\theta^2}{r^2 r_\zeta} \right) - M_{\ell\ell'}^m \left(\dfrac{1}{r_\zeta} \right) & v_m^{\ell'} \\[2ex]
+N_{\ell\ell'}^m \left(\dfrac{r^2 + r_\theta^2}{r^2 r_\zeta} \right) + L_{\ell\ell'}^m \left(\dfrac{1}{r_\zeta} \right) & w_m^{\ell'}
\end{bmatrix} =
\begin{bmatrix}
+Jc_{\ell\ell'}^m \left(\dfrac{2\Omega \zeta \sin\theta}{r} \right) & u_m^{\ell'} \\[2ex]
+L_{\ell\ell'}^m \left(\dfrac{2\Omega(r_\theta \sin\theta + r\cos\theta)}{rr_\zeta} \right) & v_m^{\ell'} \\
+N_{\ell\ell'}^m & \\[1ex]
+M_{\ell\ell'}^m \left(\dfrac{2\Omega(r_\theta \sin\theta + r\cos\theta)}{rr_\zeta} \right) & w_m^{\ell'} \\
-Mc_{\ell\ell'}^m & \\[1ex]
+M_{\ell\ell'}^m \left(\dfrac{1}{\zeta} \right) - Kc_{\ell\ell'}^m \left(\dfrac{NH_\theta}{\zeta H} \right) & \Pi_m^{\ell'} \\
-Mc_{\ell\ell'}^m \left(\dfrac{1}{\zeta} \right) & \\[1ex]
+M_{\ell\ell'}^m \left(\dfrac{1}{\zeta} \right) & \Psi_m^{\ell'} \\
-Mc_{\ell\ell'}^m \left(\dfrac{1}{\zeta} \right) & \\[1ex]
+Kc_{\ell\ell'}^m \left(\dfrac{H_\theta}{\Lambda \zeta H} \right) & b_m^{\ell'}
\end{bmatrix}.
\tag{B.12}
$$

Appendix C: The variational test

The present formulation of the variational test is the same as that of Unno et al. (1989), apart from the following differences: we use the velocity rather than the displacement, hence the extra time derivatives; the star's volume is no longer spherical; the integral on the gravity wave energy is based on the effective gravity and uses the local vertical direction rather than $\boldsymbol{e}_r$; the integral on the gravitational potential energy has been extended to infinite space.

The different resultant integrals are given by the following explicit formulas and are calculated numerically using Gauss' quadrature in the angular direction and a spectral expansion in the radial direction (we use a radial resolution

of 101 points and an angular resolution of 200 points):

$$\int_V \rho_o \|\boldsymbol{v}\|^2 dV = \int_V H^N \left[|u^\varsigma|^2 \frac{\varsigma^4}{r^4} + |u^\theta|^2 \frac{\varsigma^2(r^2 + r_\theta^2)}{r^4 r_\varsigma^2} + |u^\phi|^2 \frac{\varsigma^2}{r^2 r_\varsigma^2} + 2\Re\left\{ (u^\varsigma)^* u^\theta \right\} \frac{\varsigma^3 r_\theta}{r^4 r_\varsigma} \right] dV, \tag{C.1}$$

$$\int_V \rho_o N_o^2 |\boldsymbol{v} \cdot \boldsymbol{e}_g|^2 dV = \int_V \frac{N H^{N-1}}{\Lambda} \left(1 - \frac{\gamma}{\Gamma_1} \right) \frac{\varsigma^2}{r^4 r_\varsigma^2} \left| \varsigma u^\varsigma \partial_\varsigma H + u^\theta \partial_\theta H \right|^2 dV \tag{C.2}$$

$$\int_V \frac{|p|^2}{\rho_o c_o^2} dV = \int_V \frac{(N+1)\Lambda H^{N-1}}{\Gamma_1} |\Pi|^2 dV, \tag{C.3}$$

$$\int_V \rho_o \boldsymbol{\Omega} \cdot (\boldsymbol{v}^* \times \boldsymbol{v}) \, dV = 2i\Omega \int_V H^N \left[\left(\frac{\cos\theta}{r_\varsigma} + \frac{r_\theta \sin\theta}{rr_\varsigma} \right) \frac{\varsigma^2 \left(u_r^\theta u_i^\phi - u_r^\phi u_i^\theta \right)}{r^2 r_\varsigma} + \frac{\varsigma^3 \sin\theta \left(u_r^\varsigma u_i^\phi - u_r^\phi u_i^\varsigma \right)}{r^3 r_\varsigma} \right] dV, \tag{C.4}$$

$$\int_{V \text{ or } V_2} \|\boldsymbol{\nabla}\Psi\|^2 dV = \int_{V \text{ or } V_2} \frac{r^2 + r_\theta^2}{r^2 r_\varsigma^2} |\partial_\varsigma \Psi|^2 + \frac{1}{r^2} |\partial_\theta \Psi|^2 + \frac{1}{r^2 \sin\theta^2} |\partial_\phi \Psi|^2 - \frac{2r_\theta}{r^2 r_\varsigma} \Re \left(\partial_\varsigma \Psi^* \partial_\theta \Psi \right) dV, \tag{C.5}$$

where $dV = r^2 |r_\varsigma| \sin\theta d\theta d\varsigma d\phi$, $u_r^\varsigma = \Re\left(u^\varsigma\right)$, $u_i^\varsigma = \Im\left(u^\varsigma\right)$ etc. For the integral on the gravitational potential, it is useful to decompose infinite space into three domains: $V \cup V_2 \cup V_3 = V_\infty$. V is the volume of the star, V_2 is the volume comprised between the star and the sphere of radius 2, and V_3 is the space outside the sphere of radius 2 (see Fig. 1). The integral on the first two domains is given by the expression above. For the third domain, it is based on the spherical harmonic decomposition of the gravitational potential. In empty space, a gravitational potential will take on the following form as it obeys the equation $\Delta\Psi = 0$ and vanishes towards infinity:

$$\Psi = \sum_\ell \Psi_m^\ell Y_\ell^m = \sum_\ell \frac{A^\ell}{r^{\ell+1}} Y_\ell^m, \tag{C.6}$$

where the A^ℓ are constants. This form of Ψ then leads to the following expression:

$$\int_{V_3} \|\boldsymbol{\nabla}\Psi\|^2 dV = \sum_\ell \frac{|A^\ell|^2(\ell+1)}{r_{ext}^{2\ell+1}} = \sum_\ell r_{ext}(\ell+1) \left| \Psi_m^\ell(r_{ext}) \right|^2, \tag{C.7}$$

where $r_{ext} = 2$ is the radius of the inner sphere of V_3. This expression corresponds to the surface integral of Unno et al. (1989).